A Dynamic Unmixing Framework for Plant Production System Monitoring

Marian-Daniel Iordache, Laurent Tits, José M. Bioucas-Dias, *Member, IEEE,* Antonio Plaza, *Senior Member, IEEE,* and Ben Somers

***Abstract*—Hyperspectral remote sensing or imaging spectroscopy is an emerging technology in plant production monitoring and management. The continuous reflectance spectra allow for the intensive monitoring of biophysical and biochemical tree characteristics during growth, through for instance the use of vegetation indices. Yet, since most of the pixels in hyperspectral images are mixed, the evaluation of the actual vegetation state on the ground directly from the measured spectra is degraded by the presence of other endmembers, such as soil. Spectral unmixing, then, becomes a necessary processing step to improve the interpretation of vegetation indices. In this sense, an active research direction is based on the use of large collections of pure spectra, called spectral libraries or dictionaries, which model a wide variety of possible states of the endmembers of interest on the ground, i.e., vegetation and soil. Under the linear mixing model (LMM), the observed spectra are assumed to be linear combinations of spectra from the available dictionary. Combinatorial techniques (e.g., MESMA) and sparse regression algorithms (e.g., SUnSAL) are widely used to tackle the unmixing problem in this case. However, both combinatorial and sparse techniques benefit from appropriate library reduction strategies. In this paper, we develop a new efficient method for library reduction (or *dictionary pruning*), which exploits the fact that hyperspectral data generally lives in a lower-dimensional subspace. Specifically, we present a slight modification of the MUSIC-CSR algorithm, a two-step method which aims first at pruning the dictionary and second at infering high-quality reconstruction of the vegetation spectra on the ground (this application being called signal unmixing in remote sensing), using the pruned dictionary as input to available unmixing methods. Our goal is two-fold: 1) to obtain high-accuracy unmixing output using sparse unmixing, with low-execution time; and 2) to improve MESMA performances in terms of accuracy. Our experiments, which have been conducted in a multi-temporal case study, show that the method achieves these two goals and proposes sparse unmixing as a reliable and robust alternative to the combinatorial methods in plant production monitoring applications. We further demonstrate that the proposed methodology of combining a library pruning approach with spectral unmixing provides a solid framework for the year-round monitoring of plant production systems.**

***Index Terms*—Array signal processing, dictionary pruning, hyperspectral imaging, hyperspectral unmixing, MESMA, MUSIC-CSR, plant production systems, sparse regression, sparse unmixing, spectral libraries.**

Manuscript received September 20, 2013; revised November 26, 2013; accepted February 16, 2014. Date of publication June 23, 2014; date of current version August 01, 2014. This work was supported in part by Portuguese Science and Technology Foundation under Projects PEst-OE/EEI/LA0008/2013 and PTDC/EEI-PRO/1470/2012.

M.-D. Iordache is with the Flemish Institute for Technological Research (VITO), Centre for Remote Sensing and Earth Observation Processes (TAP), BE-2400 Mol, Belgium (e-mail: marian-daniel.iordache@vito.be).

L. Tits is with the Department of Biosystems, M3-BIORES, Katholieke Universiteit Leuven, BE-3001 Leuven, Belgium (e-mail: laurent.tits@biw.kuleuven.be).

J. M. Bioucas-Dias is with the Instituto de Telecomunicações and Instituto Superior Técnico, Universidade de Lisboa, 1049–001 Lisbon, Portugal (e-mail: bioucas@lx.it.pt).

A. Plaza is with the Hyperspectral Computing Laboratory, Department of Technology of Computers and Communications, Escuela Politécnica, University of Extremadura, Cáceres E-10071, Spain (e-mail: aplaza@unex.es).

B. Somers is with Department of Earth and Environmental Sciences, Division Forest, Nature and Landscape Research, Katholieke Universiteit Leuven, B-3001 Leuven, Belgium, and also with the Flemish Institute for Technological Research (VITO), Centre for Remote Sensing and Earth Observation Processes (TAP), BE-2400 Mol, Belgium (e-mail: ben.somers@ees.kuleuven.be).

Color versions of one or more of the figures in this paper are available online at http://ieeexplore.ieee.org.

Digital Object Identifier 10.1109/JSTARS.2014.2314960

Nomenclature

MESMA	Multiple endmember spectral mixture analysis.
SUnSAL	Sparse unmixing via variable splitting and augmented Lagrangian.
MUSIC-CSR	Hyperspectral unmixing via multiple signal classification and collaborative sparse regression.
ADMM	Alternating direction method of multipliers.
LMM	Linear mixing model.
FCLS	Fully constrained least squares.
ASC	Abundances sum-to-one constraint.
ANC	Abundances non-negativity constraint.
BPDN	Basis pursuit denoising.
OMP	Orthogonal matching pursuit.
ISMA	Iterative spectral mixture analysis.
MUSIC-SR	Hyperspectral unmixing via multiple signal classification and sparse regression.
HySime	Hyperspectral signal identification by minimum error.
CLSUnSAL	Collaborative sparse unmixing via variable splitting and augmented Lagrangian.
PBRT	Physically based ray tracer.
LAI	Leaf area index.
SMC	Soil moisture content.
SAD	Spectral angle distance.
ED	Euclidean distance.
GM1	Vegetation index whose name is composed by the initials of the authors who proposed it: Gitelson and Merzlyak.
sLAIDI	Standardized LAI determining index.
MDWI	Maximum difference water index.

I. Introduction

IN PLANT production system monitoring, the value of hyperspectral remote sensing has been amply demonstrated [1]. The spatial coverage and the ability to derive vegetation

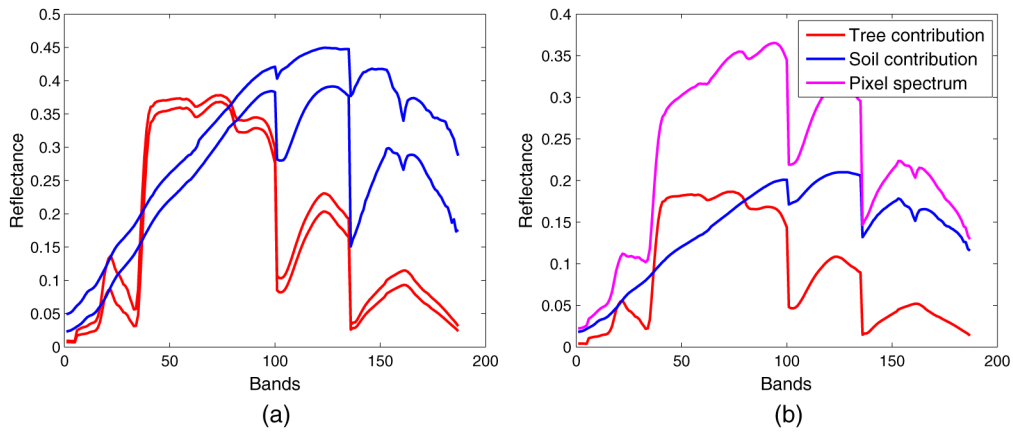

Fig. 1. Signal unmixing illustration. (a) Spectra of endmembers present in the pixel (red—tree; blue—soil). (b) Tree (red), soil (blue) signal contributions and resulting spectrum (magenta).

attributes from spectral information are important benefits. A common problem, however, is the sub-pixel spectral contribution of background soils, weeds, and shadows, which prevents the effectiveness of feature extraction (e.g., vegetation indices) to monitor site-specific variations in tree condition [2]–[4]. Mixed pixels prevail in agricultural fields due to the discontinuous open canopies, typical of most (perennial) plant production systems. The continuous monitoring of plant production systems is further complicated by temporal changes in pixel composition. Over the growing season, trees and weeds grow/decay while soil moisture conditions change depending on irrigation schemes and precipitation. These dynamic and intimately mixed scenes pose serious problems for the remote monitoring of tree condition. An accurate monitoring method for tree production parameters as such requires at all times the removal of undesired spectral background effects from the mixed image pixels [4].

Most available unmixing algorithms are focused on roughly estimating the proportional ground cover of the vegetation class (e.g., [5], [6]). This technique is popular for the rapid, early, and low-cost assessment of tree area statistics from multi-temporal and spectral low-(spatial) resolution imagery [7], [8], but the technique is clearly unable to extract spectrally pure vegetation characteristics, uncontaminated by pixel components, such as soil and shadow.

Several authors dealt with this problem partially by adjusting existing vegetation indices to make them more robust for soil background effects [9], [10]. The design of these indices is based on the assumption that soils are characterized by a unique linear relationship between near infrared (700–1350 nm) and visible (400–700 nm) reflectance, i.e., the soil line. Despite these efforts, the success of the soil-adjusted indices is limited because the soil line is not as generic as assumed [11], [12].

Consequently, a more generic approach to reduce subpixel background effects is needed. In [4] and [13], the authors proposed a *signal unmixing* methodology to extract the "pure" vegetation signal from the individual mixed pixels of a scene consisting of soil and vegetation. Fig. 1 illustrates the concept. In Fig. 1(a), two tree spectra (red) and two soil spectra (blue) contributing to one pixel are plotted. For simplicity, we assume that all endmembers contribute equally to the observed spectrum of the pixel (all have fractional abundance equal to 0.25). In Fig. 1(b), the tree signal contribution (red), soil signal contribution (blue), and the resulting spectrum of the pixel (magenta) are displayed. While classical unmixing (or area unmixing) infers fractional abundances for each of the endmembers contributing to the pixel, note that in signal unmixing we are interested in the joint spectral contribution of the endmembers of the same type [e.g., the resulting tree spectrum represented in red in Fig. 1(b)], as the quality of vegetation indices inferred directly from the observed spectrum of the pixel might be degraded by the contribution of soil signal.

The signal unmixing methodology, based on the MESMA model [14], searches for each pixel the best vegetation representative from an extended spectral library. The selected vegetation spectra are uncontaminated by undesired background effects and as such better reflect the true condition of the plant(s). Feature extraction techniques (e.g., vegetation indices) are consequently used to provide maps of plant condition parameters. Although results showed improved monitoring of site-specific variations in tree condition, the combinatorial nature of the method in combination with (the need for) large libraries provide a major bottleneck for operational implementation.

A possibly more efficient alternative for MESMA might be the unmixing algorithms that are based on the *sparsity* of the mixtures [15]–[17]. Similar to MESMA, sparse unmixing algorithms make use of large spectral libraries. The algorithms assume that the endmembers contributing to the observed spectrum of a pixel are present in the spectral library. As the number of actual endmembers on the ground is much smaller than the number of spectra in the library, the corresponding vector of fractional abundances contains only a few nonzero values, i.e., it is a sparse vector.

In recent years, a plethora of algorithms exploiting this characteristic was proposed. The unmixing is first formulated as a sparse regression problem. Then, the ADMM [18] is used to solve the obtained optimization problem. ADMM represents a class of algorithms, which decomposes a hard optimization problem into sub-problems, which are easier to solve, by introducing new variables in the objective function. The initial sparse unmixing algorithms [19] were designed to act in a *per-pixel* fashion, meaning that the unmixing solution in one pixel is considered to be independent on the solution of any other pixel in the image. Extensive tests showed that these methods outperform

the algorithms, which do not impose sparsity explixitly both in terms of accuracy and running time [20]. However, they were not used before in signal unmixing applications.

A. Library Pruning for Improved Unmixing Efficiency

As already mentioned, the use of spectral libraries opened new directions in unmixing. Originally, they were employed as an alternative to endmember extraction, given that the presence of pure pixels (for all endmembers) in the images is not ensured, most of the hyperspectral pixels being mixed due to the relative low-spatial resolution of the hyperspectral sensors [14], [21]. Also, some applications require the capture of spectral variations of one material at fine spectral level, which might not be obtained through classic endmember extraction (e.g., the detection of two distinct health states of the same type of tree in precision farming [22]). In theory, the reliability of the hyperspectral libraries improves when they contain a large number of pure signatures, as the probability of the actual endmembers on the ground to be present in the library increases. As a result, the goal is to include in the libraries as many spectra as possible. However, this leads to many drawbacks related to computational issues and to the ability of spectral unmixing algorithms to distinguish between similar signatures, as will be shown further (see also [13], [14], [21], and [23]). On the other hand, many of these signatures are not contributing at all to the observed data. From here, we can easily identify the necessity to exploit so-called library or dictionary pruning methodologies, able to retain, from a generic large library, only *useful* spectra (i.e., the ones which are likely to contribute to the observed dataset). Multiple techniques have been developed to select a reduced set of endmembers from a spectral library while capturing enough spectral variability. Different approaches have been followed (see [21] for a comprehensive overview on hyperspectral unmixing): 1) using the extreme points of the data cloud [24]; 2) minimizing of modeling error through application to a spectral library [25]; 3) minimizing of modeling error through creation of virtual endmembers [26]; or 4) optimizing of modeling accuracy [27]. These techniques were, however, designed to address endmember variability issues in spectral unmixing [28] and, therefore, target to optimize image-wide cover fraction estimate accuracies [29], [30] rather than to identify/extract the exact pure endmembers on a per-pixel basis, i.e., signal unmixing. However, a low-modeling error does not ensure the inference of the proper endmembers contributing to the observed spectrum [20]. Therefore, we propose here a new approach aiming at decoupling the pruning step from the abundance estimation by using the intrinsic low-data dimensionality characterizing the hyperspectral images, as will be shown further.

B. Toward a Dynamic Unmixing Framework for Site-Specific Monitoring of Plant Production Systems

If we want to effectively steer plant growth and plant production processes, a continuous monitoring program is required [31]. Ideally, spectral images should thus be acquired at regular moments in the growing season, as we are looking at a dynamic system with temporally variable vegetation and soil conditions. For each image, a signal unmixing procedure is needed to reduce undesired background effects and as such provide a reliable estimate of plant condition. In order to incorporate all possible plant states throughout a growing season, huge spectral databases are needed, which are subsequently used to feed combinatorial unmixing approaches, such as MESMA [13]. It is obvious, however, that the computational burden and increased ill-posedness effects related to the high collinearity between different members of the library make this signal unmixing approach infeasible to be applied in a temporal monitoring program.

In this paper, we propose a dynamic unmixing framework for the year-round site specific monitoring of plant production systems. We exploit a dictionary pruning methodology intended to remove from the spectral library (of soil and tree spectra) a significant number of signatures, which do not contribute to the observed image. The remaining pure spectra form a reduced subset of the original library (which we call pruned library or dictionary). The pruned library is then used for sparse unmixing, providing for each image pixel an estimate of the fractional abundance and pure spectral properties of the presented soil and tree components. Although it was shown that the pruning does not improve significantly the mutual coherence of the libraries (i.e., the largest cosine between any two spectral vectors in the library, which strongly influences the unmixing accuracy [18]), systematic improvements in the estimated fractional abundances were observed [32], [33]. The pure spectral properties of the trees provide sub-pixel information on the actual biophysical and biochemical condition of the trees. We recall that it is the first time that sparse unmixing is specifically implemented as a signal unmixing approach, i.e., the estimated *per-pixel* endmember spectra are considered a valuable output of the model and form the basis for sub-pixel tree condition monitoring (e.g., through vegetation indices). Traditionally, the performance of sparse unmixing is evaluated based on its accuracy to estimate the sub-pixel cover fractions. In this paper, however, we specifically focus on how well sparse unmixing is capable to provide useful sub-pixel information on tree condition. In order to evaluate the robustness and dynamic nature of our unmixing framework, we test its performance on a time series of simulated hyperspectral images over a citrus orchard covering four different periods of the growing season. The simulated images are built using ray-tracing software with in field collected canopy and soil spectra of different moments in the growing season as input. For comparison purposes, the reduced library is also used as input to MESMA, with the goal of analyzing the impact of the pruning in the unmixing performance. Note that sparse techniques were not used before in a temporal monitoring framework.

The remainder of the paper is organized as follows. Section II reviews the combinatorial and sparse regression techniques, which are used for signal unmixing. In Section III, we describe our proposed methodology for plant production systems monitoring. An extensive analysis of the quantitative and qualitative performances achieved by the method in a temporal dataset is presented in Section V. The paper concludes with a section dedicated to observations related to the proposed methodology and pointers to future work.

II. Combinatorial Versus Sparse Regression Methods in Hyperspectral Unmixing

In Section I, we have motivated the need to perform unmixing when evaluating vegetation indices, which are related to the physical characteristics of the vegetation on the ground. In this section, three unmixing algorithms related to the proposed approach are reviewed. The first one is the well-known MESMA (see [13] and the references therein), which is a combinatorial technique aimed at minimizing the reconstruction error for each observed spectrum. The second algorithm, SUnSAL [19], exploits the sparse characteristics of the spectral mixtures, on a *per-pixel* basis.

For simplicity, we establish the following terminology for the rest of the paper: an *endmember class* or, simply, *a class* denotes a specific material, structurally different from the others (e.g., soil and tree); a (library) *member* represents one spectrum of a pure material included in the spectral library (thus, it can be assigned to any of the classes); whereas a (pixel) *endmember* is a member contributing to the observed spectrum of the respective pixel.

The aforementioned algorithms assume that the LMM holds for each observed spectrum. Although nonlinearities are likely to arise in any scene, the LMM is widely used in hyperspectral applications, since, despite its simplicity, it represents a good approximation in many natural scenes. Let L be the number of spectral bands and $\mathbf{y} \in \mathbb{R}^L$ denote the L-dimensional observed spectral vector of a given pixel from a hyperspectral image. Let $\mathbf{A} := [\mathbf{a}_1, \ldots, \mathbf{a}_m] \in \mathbb{R}^{L \times m}$ denote a spectral library with m spectral signatures available *a priori*. The observed vector $\mathbf{y}$ can be expressed as a linear combination of spectral signatures taken from the library $\mathbf{A}$ as (see [20] for more details)

$$\mathbf{y} = \mathbf{A}\mathbf{x} + \mathbf{n} \tag{1}$$

where $\mathbf{x} \in \mathbb{R}^m$ is the vector collecting the fractional abundances of the m members and $\mathbf{n} \in \mathbb{R}^L$ holds the errors affecting the measurements at each spectral band.

Because the abundance fractions are non-negative and sum-to-one, the constraints $\mathbf{x} \geq \mathbf{0}$ (to be understood in the component-wise sense) and $\mathbf{1}_m^T \mathbf{x} = 1$ ($\mathbf{1}_m$ stands for a column vector with m ones) called abundance non-negativity constraint (ANC) and abundance sum-to-one constraint (ASC), respectively, are often imposed into the model (1).

A. Multiple Endmember Spectral Mixture Analysis

MESMA is a widely used combinatorial method to estimate fractional abundances of the endmembers in a given scene. Let us suppose that the spectral library $\mathbf{A}$ contains pure spectra of distinct classes. For each observed spectral vector $\mathbf{y}$, MESMA generates combinations of endmembers belonging to distinct classes and then performs FCLS [34] unmixing, expressed as the following optimization problem:

$$\min_{\mathbf{x}_t} \|\mathbf{A}_t \mathbf{x}_t - \mathbf{y}\|_2^2 \text{ subject to: } \mathbf{x}_t \geq 0,\ \mathbf{1}_t^T \mathbf{x}_t = 1 \tag{2}$$

where $\mathbf{A}_t$ is the matrix composed by the selected members (a small subset of $\mathbf{A}$); $\mathbf{x}_t$ is the vector of fractional abundances compatible with $\mathbf{A}_t$; and $\mathbf{1}_t$ is a vector of ones with t components.

The optimization problem (2) infers a solution vector $\mathbf{x}_t$, which minimizes the reconstruction error of the observed pixel, provided that the abundances satisfy the ASC and the ANC. From all the spectra combinations evaluated, MESMA retains, as a final solution, the one with the lowest reconstruction error. Although this strategy leads to satisfactory results, it is subject to two major drawbacks: 1) the number of possible spectra combinations is combinatorial, with makes an exhaustive search impossible as the number of classes increases; and 2) due to time constraints, not all the possible combinations can be evaluated; usually, a fixed number of tests is performed, which decreases the probability of finding the correct endmembers [13]. Moreover, MESMA typically enforces the presence of exactly one endmember from each class, which might force the solution to contain endmembers, which are not in the mixture or, contrarily, to lack ground-truth endmembers, if the pixel contains more than one endmember belonging to the same class.

B. Sparse Unmixing via Variable Splitting and Augmented Lagrangian

Sparse regression opened recently many alternatives to classical unmixing algorithms. The sparse unmixing techniques exploit the fact that one pixel contains a relative low number of endmembers, compared to the number of pure spectra contained in the library. The estimated vector of fractional abundances is, then, a sparse vector, as all the members, which are not present in mixed pixels should have null abundances. The goal of sparse unmixing is to find a reduced set of endmembers present in the mixture, which reconstructs the observed pixel with high accuracy.

The performances of sparse unmixing techniques are affected by several factors, such as the cardinality of the solution (number of active endmembers), the mutual coherence of the spectral library (i.e., the maximum value of the cosine between any two columns: $\mu(\mathbf{A}) \equiv \max_{1 \leq k,j \leq m,\ k \neq j} \frac{|\mathbf{a}_k^T \mathbf{a}_j|}{\|\mathbf{a}_k\|_2 \|\mathbf{a}_j\|_2}$) [35]–[38] and the number of spectral signatures in the library, among others [20]. In an ideal case, the unmixing should involve highly sparse mixtures and spectral libraries with low coherence. In practice, the former observation is generally true (the cardinality of the solution vector is usually low), but the latter is not (the mutual coherence of real spectral libraries is often close to one), which leads to difficulties due to the high similarity between distinct pure signatures. Even so, it was shown that sparse regression can partially overcome these limitations [20].

In a sparse regression framework, the unmixing can be formulated as an optimization problem as follows:

$$\min_{\mathbf{x}} \|\mathbf{x}\|_0 \text{ subject to } \mathbf{A}\mathbf{x} = \mathbf{y} \tag{3}$$

where the so-called ℓ_0-norm simply counts the nonzero components in $\mathbf{x}$. In other words, we seek for the smallest set of library spectra, which perfectly explains the observed data.

The optimization problem (3) is nonconvex and combinatorial, hard to solve [39]. In practice, the ℓ_0-norm is relaxed to the ℓ_1-norm, which was shown to produce similar results under certain conditions of coherence [40]. Moreover, because of the existence of noise, the observed spectrum cannot be exactly

recovered in practice, thus, a small reconstruction error δ should be allowed. The optimization problem (3) becomes, then, the so-called BPDN problem [41]

$$\min_{\mathbf{x}} \|\mathbf{x}\|_1 \text{ subject to } \|\mathbf{A}\mathbf{x}-\mathbf{y}\|_2 \leq \delta \tag{4}$$

which can be re-expressed, by incorporating the constraint into the objective function

$$\min_{\mathbf{x}} \frac{1}{2}\|\mathbf{A}\mathbf{x}-\mathbf{y}\|_2^2 + \lambda\|\mathbf{x}\|_1. \tag{5}$$

In (5), the first term is the data fidelity term and the second term imposes sparsity, while $\lambda \geq 0$ is a regularization parameter, which weights the two terms of the objective function (or the Lagrangian multiplier). To solve the optimization problem (5), we use the SUnSAL algorithm,[1] which is a fast algorithm specifically designed for hyperspectral scenes. Based on ADMM, SUnSAL is able to incorporate both the ANC and the ASC. In our experiments, we employ ANC only, as, when ASC is enforced in the optimization problem (5), the second term plays no role and the solution of the unmixing is equivalent to the classical FCLS solution. For a detailed assessment on the superiority of SUnSAL over techniques, which do not enforce sparsity explicitly (such as OMP [42] and ISMA [43]), see [20].

SUnSAL is a *per-pixel* sparse unmixing algorithm specifically designed for hyperspectral applications. Inspired by SUnSAL, recent developments opened new perspectives in unmixing, by exploiting the intrinsic group structure of the spectral libraries [44], the relative low number of endmembers that contribute to the data in a collaborative way [45] (sparsity across the pixels) or the piece-wise smooth spatial distribution of the endmembers [46], [47].

III. MUSIC-CSR and Proposed Adaptation for Plant Production System Monitoring

MUSIC-CSR is a two-step unmixing algorithm, which exploits the fact that the observed vectors share the same support in order to obtain accurate fractional abundances. The first step, similar to the MUSIC array signal processing algorithm [48], [49], selects, from the available library, a subset of pure spectra suitable to represent the observed dataset. Consequently, the second step applies collaborative sparse regression CSR to the reduced library. CSR is intended to promote sparsity across the pixels, which results in a matrix of abundance fractions with only a few nonzero lines. This means that one single member from the library can explain many pixels in the observed dataset. This is an aspect that we do not specifically encourage in our application, as we aim at capturing fine spectral differences between different pixels. This is why we replace the second step of MUSIC-CSR with the per-pixel processing techniques detailed in Section II: SUnSAL and MESMA. Such modified version of MUSIC-CSR is called MUSIC-SR, where SR stands for *sparse regression*. Although MESMA does not impose the sparsity of the solution explicitly (i.e., it does not include a sparse regularizer in the objective function), it still returns a sparse solution (where the number of nonzero components in the fractional abundances vector is always equal to the number of endmember classes.)

The modalities of the MUSIC-CSR algorithm and the underlying principles are detailed in [32]. The MUSIC-SR algorithm, shown in Algorithm 1, uses literally the pruning part of MUSIC-CSR. The input is represented by the spectral library $\mathbf{A}$, the hyperspectral image $\mathbf{Y} \in \mathbb{R}^{L\times N}$, the number of signatures to be retained r and the regularization parameter λ used in the SR optimization problem (5) in which the ANC constraint is usually imposed. If MESMA is employed in the unmixing step, this regularization parameter does not apply. The algorithm returns a reduced set of signatures collected in the matrix $\mathbf{A}_R$ and the fractional abundances corresponding to the reduced set, collected in the matrix denoted by $\mathbf{X}^R$.

Algorithm 1: MUSIC-CR

Input: $\mathbf{A} \in \mathbb{R}^{L\times m}$ (library), $\mathbf{Y} \in \mathbb{R}^{L\times n}$ (hyperspectral image), r (number of signatures to be retained), λ (regularization parameter)

Output: $\mathbf{A}_R$ (detected signatures), $\mathbf{X}^R$ (fractional abundances with respect to $\mathbf{A}_R$)

1 **begin**

2 $\mathbf{E} := \text{HySime}(\mathbf{Y})$ (estimate an orthonormal basis for $\text{range}(\mathbf{A}_S)$ using the HySime algorithm [50])

3 $\mathbf{P}^{\perp}_{\mathbf{A}_S} := \mathbf{I} - \mathbf{E}\mathbf{E}^T$ (projector on $\text{range}(\mathbf{A}_S^{\perp})$)

4 **for** $j = 1$ **to** m **do**

5 $\varepsilon_j := \frac{\|\mathbf{P}^{\perp}_{\mathbf{A}_S}\mathbf{a}_j\|_2}{\|\mathbf{a}_j\|_2}$

6 $\pi := \text{permutation}\{1,\ldots,n : \varepsilon_{\pi(i)} \leq \varepsilon_{\pi(j)}, i \leq j\}$

7 $R := \{\pi(i), i = 1,\ldots,r\}$

8 Perform unmixing using SUnSAL [19] or MESMA, [14] using the pruned library $\mathbf{A}_R$.

The two parts of the MUSIC-SR are performed as follows. Steps 2)–7) of the algorithm select, from the original library, a set of pure signatures linked to the subspace in which the data lives. The data subspace is estimated in Step 2), using the HySime algorithm[2] [50], which is fully automatic (it does not require input parameters). The algorithm provides a set of eigenvectors to define the data subspace and also estimates the number of endmembers in the image k. In step 4), the EDs from each library member to the estimated subspace are computed through the orthogonal projector $\mathbf{P}^{\perp}_{\mathbf{A}_S} := \mathbf{I} - \mathbf{E}\mathbf{E}^T$ computed in Step 3). Steps 6) and 7) sort, in increasing order, the normalized projection errors computed in the previous step and retain, from the original library, the spectra corresponding to the first r of them, respectively. In other words, the library spectra that are the closest in terms of ED to the data subspace are retained in the pruned library. Ideally, they should lie in the data subspace, but it is not always the case in real applications, due to acquisition and

[1]Available online: http://www.lx.it.pt/bioucas/publications.html.

[2]Available online: http://www.lx.it.pt/bioucas/code.htm.

modeling errors. Note that, in this paper, we will adopt a conservative approach, by retaining a number of r pure spectra, where $r > k$ and $k_f > k$ eigenvectors to define the data subspace, in order to ensure that the subspace representation is only weakly affected by measurement errors (noise). In our application, we retain r_1 tree spectra and r_2 soil spectra, leading to a total of $r = r_1 + r_2$ with $k < r$. Step 8) represents the second part of the MUSIC-CR algorithm, i.e., the unmixing process w.r.t. the selected subset of spectra, using one of the algorithms described in Section II. As previously mentioned, the original unmixing algorithm used in MUSIC-CSR, called CLSUnSAL [45], is replaced, in turn, by MESMA and SUnSAL algorithms. This is due to the fact that we are more interested in exploiting the variability of the signatures rather than in encouraging dominant endmembers. In our application, we are very interested in the pruning strategy, which is likely to increase the probability to find correct solutions, but we feel that by constraining the estimated matrix of fractional abundances to contain a small number of nonzero lines might result in a weak capacity of the algorithm to capture fine spectral variations from one pixel to another. It results that the per-pixel processing, to which MESMA and SUnSAL belong, is more appropriate than the collaborative approach in this specific application.

IV. Experimental Setup

This section describes the temporal dataset used in the experiments and the performance discriminators employed for an extensive qualitative and quantitative assessment.

A. Simulated Dataset

Here, we detail the data used in our experiments: ground-truth spectra, spectral libraries, and simulated images.

1) Virtual Orchard: The synthetic hyperspectral image data considered in this work were generated from a ray-tracing experiment in a fully calibrated virtual citrus orchard using the PBRT model [51]. With this type of data, the complexity of real hyperspectral images can be simulated, implicitly incorporating effects such as multiple photon scattering and shadowing/shading effects. In addition, the reference data can be exactly derived, as such allowing an objective and extensive evaluation of the methodology [52]. In the virtual orchard, 10 different 3-D representations of citrus trees were created based on the triangular mesh algorithm described in [53]. The spectral interactions between the photons and the components in the scene (i.e., leaves, branches, stems, and soil) as well as the atmosphere were modeled realistically using bidirectional reflectance distribution function models and sky maps [51]. The scene illumination was simulated using the combination of two light sources: a directional light source for the direct (unscattered) light and a skymap that contains the angular distribution of diffuse light.

2) Spectral Measurements: The spectral properties of the different components were determined based on field measurements. *In situ* measured spectral data were collected in a citrus orchard near Wellington, South Africa ($33°35'0''$ and $18°55'30''$), the same orchard used to calibrate the virtual orchard [51], [54]. The orchard block had a row spacing of 4.5 m, a tree spacing of 2 m and a row azimuth of $7.3°$. The average tree height was 3 m. The soil between the trees was classified as "Albic Luvisols" (FAO, 1998), and had a sandy texture with an average organic content of 0.53% [12]. Spectral measurements were collected within one hour of local solar noon on clear sky days using a full-range (350–2500 nm) spectroradiometer (ASD®, Boulder, CO) with a $25°$ foreoptic.

TABLE I
Solar Positions at the Orchard for Four Different Dates

Time	Solar elevation (°)	Solar azimuth (°)
December 22	79.2	339.6
March 21	56.4	356.4
June 21	32.8	356.1
October 10	40.54	356.6

During a two year period, monthly spectral measurements were taken of the soil, canopy, and leaves [54]. As such, seasonal changes in phenology (e.g., new shoot growth, blossoming, fruit formation, harvest, and pruning) were incorporated. Soil measurements were taken from nadir at a height of 1 m above the surface, while tree canopy spectra were measured at 2 m above the tree top. Leaf spectral measurements were taken from randomly selected leaves in the top of the canopy. In addition to the spectral measurements of the different components in the orchard, skymaps were generated for different solar elevations and azimuths that correspond to four different points in time. An overview of the dates and the corresponding solar positions is given in Table I.

3) Scenarios: From the extensive spectral dataset consisting of the monthly measurements, the measurements closest to the dates of the skymaps were selected. The leaf reflectance measurements were inverted using the PROSPECT model [55] to estimate leaf structure and biochemical composition (e.g., pigmentation, and water content). The transmittance was obtained by running the model again in the forward mode [51]. To incorporate different stresses in the orchard, the biochemical composition of the leaves was altered before running PROSPECT in the forward mode. The chlorophyll content of the leaves was reduced to 50%, and the water content of the leaves to 70%. In addition, from the 3-D geometries of the trees, leaves were randomly removed to obtain trees with an LAI around 56% of the reference trees. As such, four different orchards could be generated for each time period (i.e., reference, chlorophyll stress, water stress, and LAI stress). For the creation of each orchard, 10 different tree geometries were available. With these trees, the orchards were constructed by randomly repeating the trees throughout the orchard.

Six different regions were defined in each of the orchards to incorporate spatial variability in soil moisture throughout the orchard. In the summer month (December), a low-SMC was implemented, ranging between 0 and 10% gravimetric SMC. For spring and autumn (March and October), the SMC ranged between 10% and 20%, whereas in the winter, the SMC ranged between 20 and 30%. A hyperspectral image of each of the 16 orchards (four stresses and four time periods) was generated in

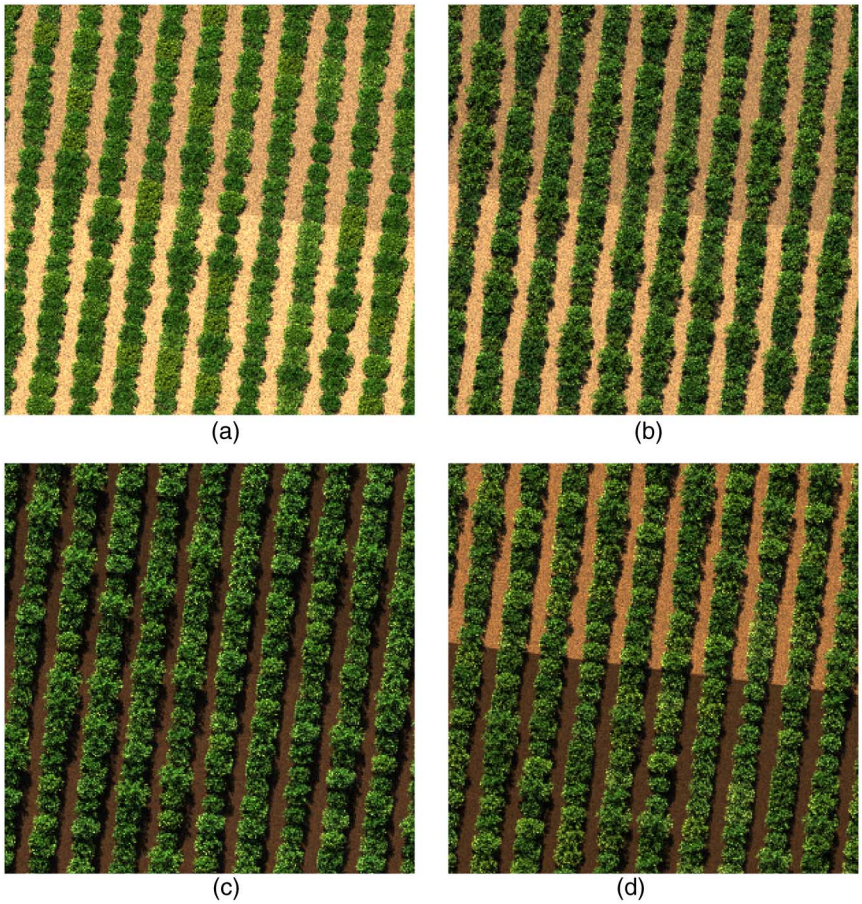

Fig. 2. RGB images of the orchard along the four seasons: (a) January, (b) March, (c) June, and (d) September.

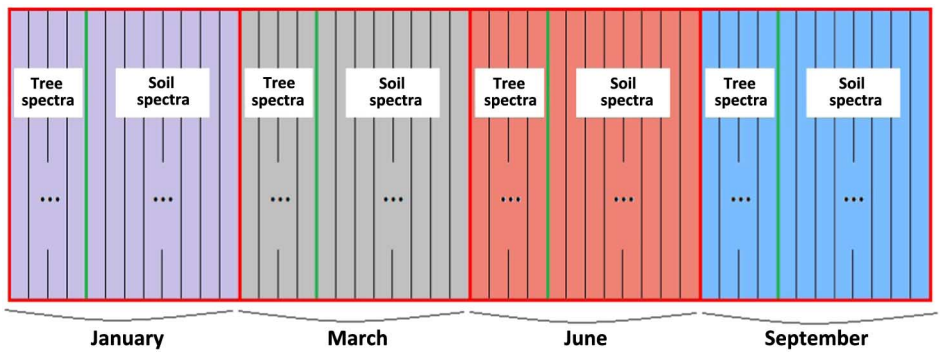

Fig. 3. Library organization. Each color represents spectra contributing to the observed scene in one specific season. In each season, there are 40 tree and 540 soil ground-truth spectra.

the ray-tracer, with a spatial resolution of 2 m to simulate an airborne sensor. The spectral range was 350–2500 nm, with a spectral resolution of 10 nm.

For illustrative purposes, we show, in Fig. 2, RGB images of the four simulated datasets. Note that, despite the data are simulated, most of the parameters affecting the observation of natural scenes (e.g., nonlinearities, shadows, and multiple scattering) are taken into account, which leads to a very accurate modeling of a real plant production system. Another advantage of the simulated dataset used in our experiments is the control, which we have on the scene parameters, which allows us a detailed assessment of the performances of the proposed method, this being nearly impossible using real data due to the actual difficulties in acquiring ground-truth information on a temporal basis.

4) Spectral Libraries: The reference canopy and soil spectra from all seasons were compiled in the spectral library $\mathbf{A} \in \mathbb{R}^{216\times 2320}$, containing 2320 spectra measured in 216 spectral bands with nominal spectral resolution of 10 nm. Note that, from this library, only 580 spectra (40 tree spectra and 540 soil spectra) are contributing to each season separately, whereas the others can be regarded as extra spectra. The organization of the library is schematically represented in Fig. 3, in which each color represents the spectra generating the dataset corresponding to one specific season.

B. Performance Discriminators

We explore the capabilities of the proposed method from two viewpoints. 1) The ability to retain correct endmembers from the initial spectral library in the dictionary pruning step is tested in various scenarios. 2) The quality of the reconstructed vegetation spectra on the ground is measured in terms of the $\mathrm{SAD}(\mathbf{x}_1, \mathbf{x}_2) = \arccos(\frac{\mathbf{x}_1^T \mathbf{x}_2}{\|\mathbf{x}_1\|_2 \|\mathbf{x}_2\|_2})$ between the true spectrum and the reconstructed spectrum obtained after the unmixing. At the same time, we measure the ED $(\mathrm{ED}(\mathbf{y}_1, \mathbf{y}_2) = \sqrt{\Sigma_{i=1}^{L} (\mathbf{y}_{1,i} - \mathbf{y}_{2,i})^2})$ between the normalized true and reconstructed spectra and we report the average value over all pixels. Note that, from the point of view of the vegetation indices computation, SAD is more informative than the ED, as it is invariant to illumination factors. The running times of the algorithms are also specified. An illustration of the quality of inferred vegetation indices in two cases: before and after dictionary pruning and spectral unmixing, is also included. The three vegetation indices taken into account are:

1) GM1 [56] index: $\mathrm{GM1} = \frac{R_{750}}{R_{550}}$, where R_{750} and R_{550} are the reflectances registered at the wavelengths $\lambda_1 = 750$ and $\lambda_2 = 550$ nm, respectively.
2) The standardized LAI Determining Index [57]: $\mathrm{sLAIDI} = S \cdot \frac{R_{1050} - R_{1250}}{R_{1050} + R_{1250}} \cdot R_{1555}$, where R_{1050}, R_{1250}, and R_{1555} are the reflectance values measured at the respective wavelengths and S is a scaling factor to rescale the index between 0 and 1, equal to 40.
3) The maximum difference water index [58]: $\mathrm{MDWI} = \frac{R_{max}(1500-1750) - R_{min}(1500-1750)}{R_{max}(1500-1750) + R_{min}(1500-1750)}$, where $R_{max}(1500 - 1750)$ is the maximum reflectance in the wavelength interval 1500–1750 nm and $R_{min}(1500 - 1750)$ is the minimum reflectance in the same interval of wavelengths.

These indices are adopted due to their versatility in characterizing the health parameters of the vegetation (i.e., chlorophyll content, LAI and leaf water content, respectively). They were previously tested by other authors in several scenarios (see, e.g., [57], [59], and [60]), being shown that they exhibit a good correlation to the actual health state of the vegetation on the ground, especially in Citrus orchards [61].

We analyze several scenarios related to the input library, dimensionality of the subspace and the number of selected spectra. First, we assume that the library is formed by the collection of true ground spectra over the four seasons, with the goal to check the accuracy of the pruning method in selecting correct spectra related to each specific season. Then, the library is extended with spectra which do not contribute to the image. In this case, the selection process is expected to become more difficult, due to the extra variability induced. The number of eigenvectors retained from the HySime output to define the data subspace, denoted by k_f, takes the following values: $k + 20$, $k + 35$, and $k + 50$, where k defines the dimension of the subspace in which the data lives, infered by the same algorithm. Finally, two situations regarding the number of selected spectra are investigated: in the first case, we assume that we know the correct number of tree and soil spectra contributing to the observed image; then, in a general setup, we set the number of selected tree and soil signatures to different empirical levels (60 and 100 spectra, respectively, for both tree and soil).

V. Experimental Results

This section analyzes the performance of the proposed method, according to the experimental setup described in Section IV. In Section V-A, we provide a qualitative and quantitative assessment of the pruning process w.r.t. the number of correct spectra retained in several configurations and the ability to properly cover the variability range of the ground-truth endmembers. The accuracy of the reconstructed vegetation spectra is investigated next. A comparison of the running times of the considered algorithms under different conditions is also presented. Section V-B illustrates the potential of the proposed method to infer accurate vegetation indices. To evaluate the robustness of the pruning method new members, which are not contributing to the observed data, are added to the spectral library, and the tests related to the pruning strategy are repeated. Section V-C is devoted to a short discussion on the obtained results.

A. Accuracy of the Dictionary Pruning Process

Table II shows the number of correctly retained spectra by the proposed method, for all the considered datasets and simulation conditions, when the original library is pruned by setting r_1 and r_2 to different values. Note that the correct spectra might not be necessarily mandatory for obtaining accurate reconstructions of the observed vegetation spectra. However, we consider that this indicator is crucial for analyzing the accuracy of the pruning step, given that the selection of true endmembers should further guide the unmixing toward more accurate solutions. On the other hand, the matching of a dataset to a certain season can be considered a fast and simple application of the pruning step—the data is likely to be acquired during the season to which the retained spectra correspond.

From Table II, it can be easily seen that the pruning methodology is able to select (with relative high accuracy) correct spectra from the library. In all cases, most of the tree spectra contributing to the actual observed dataset were selected. In the first case, which corresponds to the situation when the number of true spectra on the ground is available, the algorithm misses a part of the actual spectra. We will analyze later if or how this situation influences the accuracy of the reconstructed vegetation spectra. However, when r_1 increases, less vegetation spectra are missed in the pruned library (note that, when $r_1 = 100$, all the true tree spectra are correctly selected). Regarding the soil spectra, we can conclude that the pruning is more accurate when the number of eigenvectors defining the subspace is not too low (see the lines corresponding to $k_f = k + 20$ versus the ones corresponding to $k_f = k + 35$). However, when k_f is even more increased (e.g., $k_f = k + 50$), no improvements are observed. We can see now why the conservative approach adopted here, in which the data subspace is defined by a number of eigenvectors larger than the number of endmembers inferred by HySime and the number of retained spectra is preferably set to relative high values, is indeed necessary.

For illustrative purposes, we plot, Fig. 4(a) plots the projection errors, for all library members, when $k_f = k + 50$, $r_1 = 40$, and

TABLE II
NUMBER OF CORRECTLY IDENTIFIED SPECTRA IN CONSIDERED SCENARIOS

Retained spectra Tree	Retained spectra Soil	Subspace dimension	Type of retained endmember	January ($k = 10$)	March ($k = 10$)	June ($k = 12$)	September ($k = 10$)
$r_1 = 40$	$r_2 = 540$	$k_f = k + 20$	Tree	32	32	30	35
			Soil	380	322	540	540
		$k_f = k + 35$	Tree	40	32	32	35
			Soil	402	448	540	540
		$k_f = k + 50$	Tree	40	33	32	34
			Soil	398	448	540	540
$r_1 = 60$	$r_2 = 60$	$k_f = k + 20$	Tree	38	39	36	40
			Soil	56	60	60	60
		$k_f = k + 35$	Tree	40	36	38	40
			Soil	60	60	60	60
		$k_f = k + 50$	Tree	40	36	38	40
			Soil	60	60	60	60
$r_1 = 100$	$r_2 = 100$	$k_f = k + 20$	Tree	40	40	40	40
			Soil	96	100	100	100
		$k_f = k + 35$	Tree	40	40	40	40
			Soil	100	100	100	100
		$k_f = k + 50$	Tree	40	40	40	40
			Soil	100	100	100	100

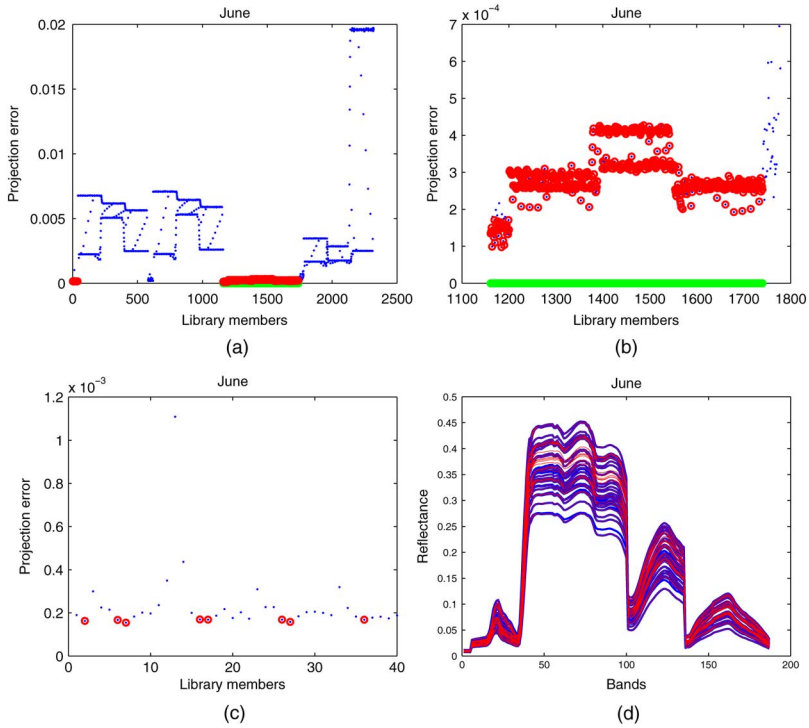

Fig. 4. (a)–(c) Projection errors corresponding to the library members in the June dataset. Green circles represent the true endmembers. Red circles correspond to the projection errors of the 580 selected spectra (40 soil spectra and 540 tree spectra). (a) Projection errors, actual members and selected members. (b) Correctly selected members. (c) Erroneously selected members. (d) Selected and ground-truth spectra.

$r_2 = 540$, in the June dataset. The green circles correspond to actual endmembers on the ground and the red circles mark the projection errors of the selected spectra. A zoom on the regions of interest (i.e., the ones which contribute to the pruned library due to the low-projection error of the members) is shown in Fig. 4(b) and (c). Note that all the soil signatures corresponding to actual spectra on the ground are correctly selected in the pruning process. Regarding the tree signatures, there are eight spectra which are missed by the pruning, with others being selected instead. In Fig. 4(d), we plot the set of ground-truth spectra (blue), jointly with the set of selected spectra (red). Note that the selected spectra cover satisfactorily the whole range of

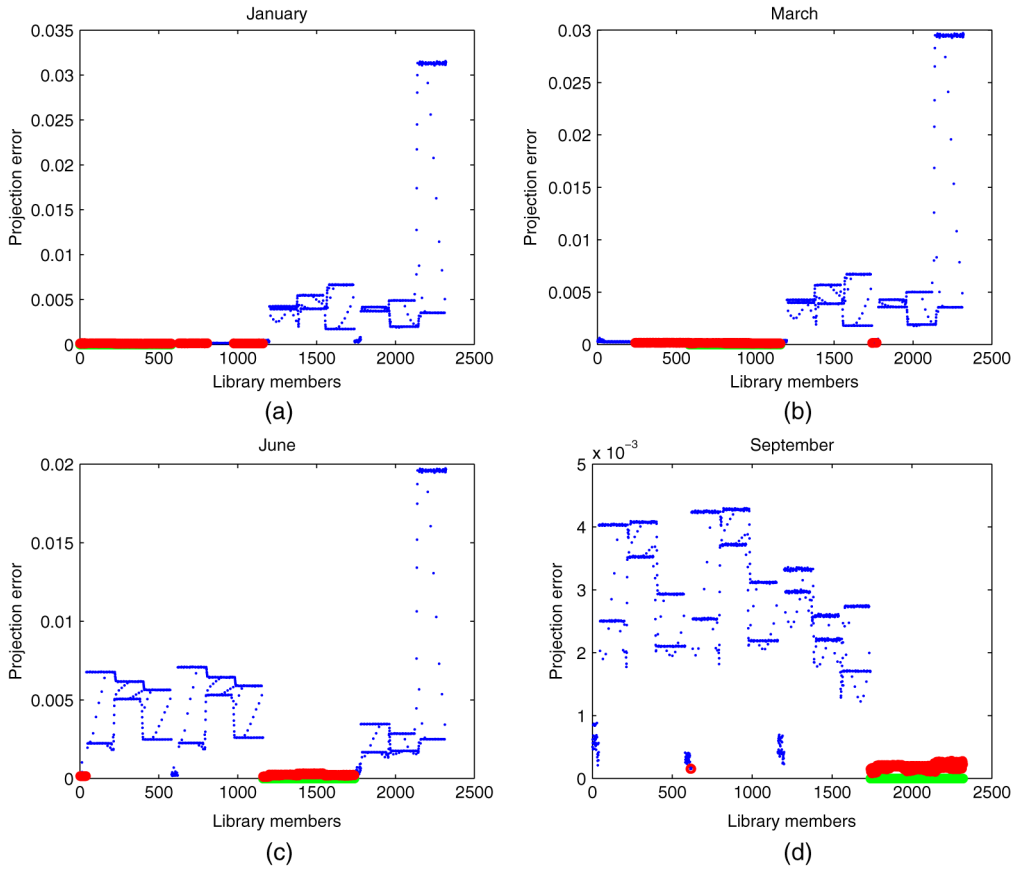

Fig. 5. Projection errors corresponding to each library member in the considered datasets. Green circles represent the true endmembers. Red circles correspond to the projection errors of the 580 selected spectra (40 soil spectra and 540 tree spectra). (a) January, (b) March, (c) June, and (d) September.

variability of the ground-truth spectra. This is encouraging, as it shows that the spectra incorrectly selected are similar to the actual ones, which is expected to have only a weak impact on the quality of the unmixing. The set of 580 selected spectra composes the spectral library which is then used in unmixing.

Another perspective on the accuracy of the pruning step is presented in Fig. 5, which shows, in a similar fashion to Fig. 4, the selected spectra when $k_f = k + 100$, $r_1 = 40$, and $r_2 = 540$, for all images. Note that, by relating Fig. 5 with Fig. 3, it is easy to infer in which season the data were acquired, as most of the selected members always belong to the correct library subset. A stronger confusion between the soil signatures from January and March is visible, due to the similiarity of the soil conditions in these 2 months. From Fig. 5, the fine sensitivity of the dictionary pruning step to the variations of the data subspace is clearly proved due to the visible differences appearing between the projection errors corresponding to the same member (especially for soils) in distinct datasets.

B. Proper Coverage of the Spectral Variability

An important issue is to establish how accurately the selected spectra can cover the variability of the tree signatures in each season. For a qualitative comparison, we plot, in Fig. 6, the following features: the variability range of the spectral library (blue area), the variability range of the tree signatures in the corresponding season (green area), and the selected signatures after the pruning step (magenta).

From Fig. 6, it can be easily seen that the selected signatures cover satisfactorily the variability range of tree signatures on the ground. A very interesting case is the June dataset, in which the actual tree signatures cover the entire spectral variability of the tree library. Even in this case, the selected signatures are able to cover the entire variability range. The plots corresponding to the other three datasets confirm the accuracy of the member selection process (note how the selected signatures follow closely the distribution of the actual spectra on the ground, depending on the specific season).

C. Accuracy of the Reconstructed Vegetation Spectra

In this section, the quality of the reconstructed vegetation spectra is investigated in terms of SAD and ED. In the experiments, the pruned libraries with $r_1 = 40$ and $r_2 = 540$ spectra obtained by dictionary pruning when $k_f = k + 35$ are used as input for MESMA and SUnSAL. Fig. 7 shows the plots of SAD (left column) and ED (right column) w.r.t. the number of iterations (for MESMA, on the superior x-axis, colored in red) and the regularization parameter λ (for SUnSAL, on the inferior x-axis, colored in blue). In these plots, values obtained after MESMA-based unmixing are plotted in red (continuous line for the full library and dashed line for the pruned library), while the ones corresponding to SUnSAL are plotted in blue. The number of iterations for MESMA varies between 10 and 200, while λ takes values between 0 [which leads to the classical non-negative least-squares (NCLS) solution] and 0.05.

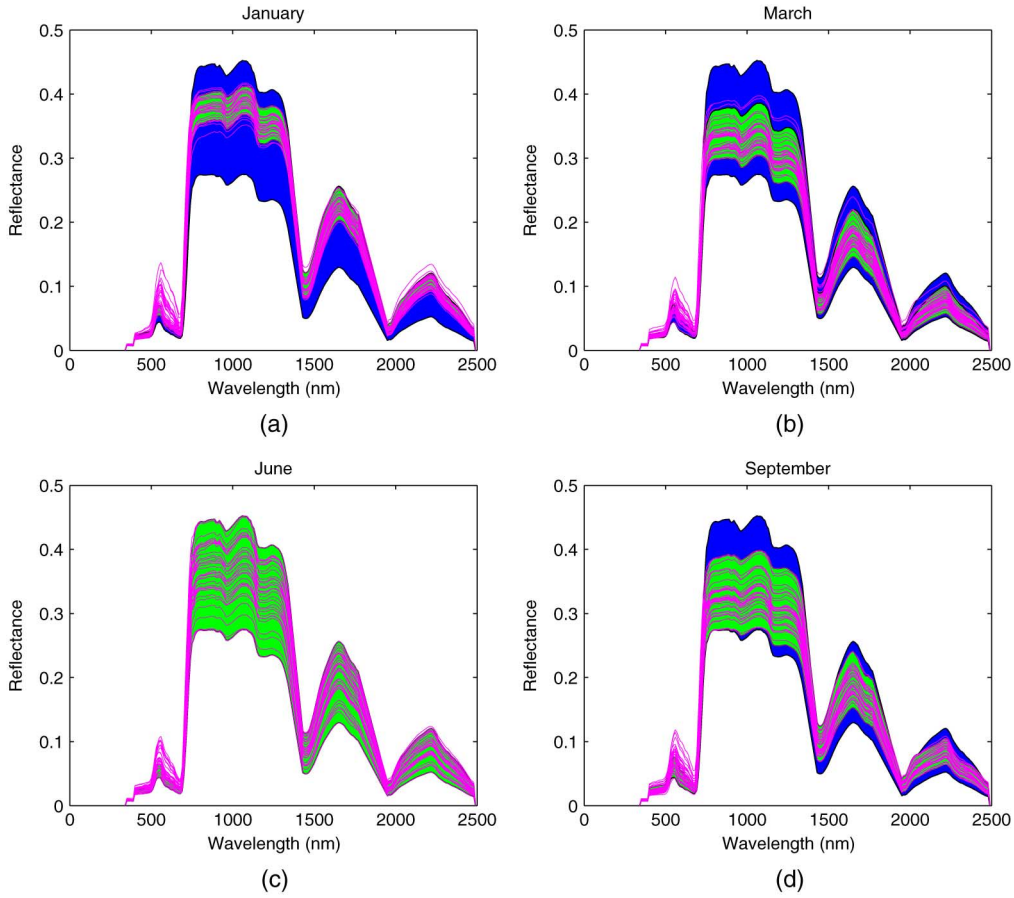

Fig. 6. Quality of the variability range coverage for the four seasons (blue: range of the tree library signatures; green: range of the tree signatures in the specific season; magenta: selected tree signatures through library pruning). (a) January, (b) March, (c) June, and (d) September.

From Fig. 7, a few important observations can be drawn. It is useful to note that, most of the times, MESMA exhibits the tendency to converge to the same average SAD and ED values, independently of the library used, which proves that the pruning does not have a negative impact on the performance. The difference between the two situations (full and pruned library, respectively) is that MESMA exhibits a smoother performance, no matter the number of iterations, when the pruned library is employed. On the other hand, when the full library is used, the algorithm needs more iterations to achieve improved performance (usually, at least 100 iterations). This means that, by dictionary pruning, the reliability of MESMA output is greatly improved when a low number of iterations is conducted, which is useful in an operational approach, i.e., when the running time is limited. Note the important improvements achieved by MESMA when the number of iterations is set to a low value, say only 10. On the other hand, sparse unmixing is able to improve both the SAD and ED between the estimated and true vegetation spectra in all considered scenarios. We can conclude, then, that sparse unmixing with pruned libraries is able to achive generally better performances than MESMA, irrespectively of the scene considered in the experiments.

D. Algorithms Comparison w.r.t. the Running Times

Table III reports the running times of the proposed technique. From our experience, the library pruning part [Steps 2)–7) in Algorithm 1] has negligible running time variation when the number of retained eigenvectors k is varied. This is why we consider only the specific case when $k = k_f + 35$. The same observation is valid for SUnSAL in what concerns the regularization parameter λ, for which we consider the value 0.005 as a reference. The running time of MESMA is also relatively stable for a fixed number of iterations. From our previous experiments, we can conclude that MESMA obtains satisfactory results after at least 100 iterations with the full library and after 50 iterations with the pruned library, thus we report the total running times obtained in these two situations (obviously, the running time *per iteration* is comparable in the two cases). This setup is conceived such that the algorithms compete under similar conditions of required accuracy.

Table III reveals that the dictionary pruning step has negligible running time (less than one second). MESMA running with the full library exhibits a very large running time. For a similar accuracy, the running time decreases proportionally with the reduction in the number of spectra obtained through dictionary pruning. However, SUnSAL requires a very low-execution time compared to MESMA, which, correlated to the high quality of the reconstructed spectra, proposes sparse unmixing as a powerful alternative to the combinatorial approach in the year-round site specific monitoring of plant production systems. Section V-E shows a concrete illustration of the improvements brought by the proposed technique to evaluating specific vegetation indices in this context.

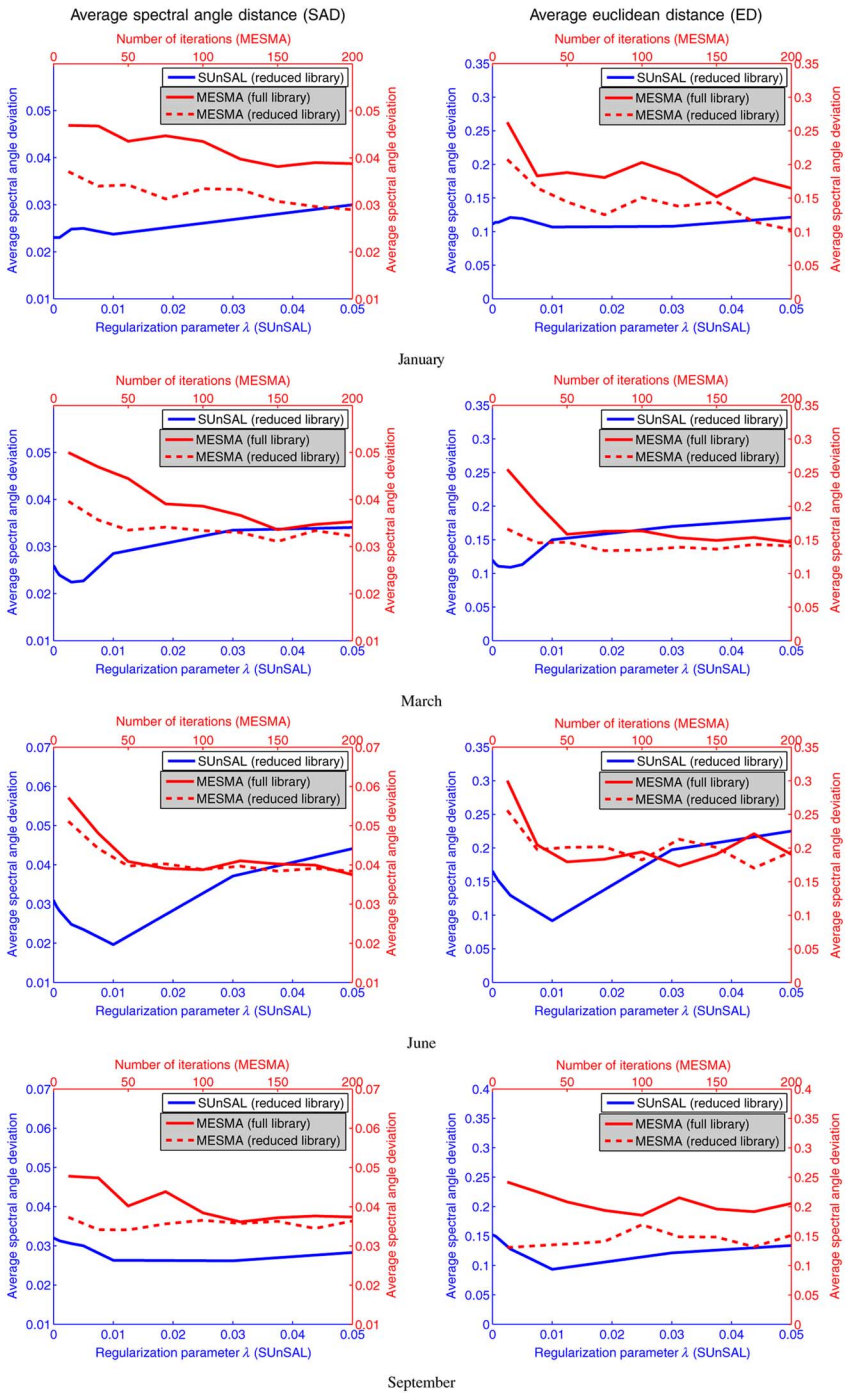

Fig. 7. Plots of the average SAD (left column) and average ED (right column) between the reconstructed and the true vegetation spectra in different scenarios. Each row of plots corresponds to one month of the year. The results are based on a pruned library with 540 members (40 tree spectra and 540 soil spectra) when the number of eigenvectors to define the data subspace is set to $k_f = k + 35$.

E. Illustrative Evaluation of Vegetation Indices

In this section, we compute a series of vegetation indices with the goal to analyze the influence of the proposed method on the quality of the inferred values. The vegetation indices employed here are the three indices introduced in Section IV-B.

First, we provide a qualitative assessment of the estimated indices. Figs. 8–10 show, respectively, the maps for the three considered indices (GM1, sLAIDI, and MDWI), in all seasons. In each figure, the first column displays the ground-truth values of the respective index, computed from the original vegetation spectrum. The second column shows the index maps resulting directly from the observed dataset (mixed pixels). The following columns show the estimated maps of the considered index, computed, in turn, by the following algorithms: MESMA running with full library and 200 iterations (Mf200), MESMA using pruned library and 50 iterations (Mp50) and SUnSAL (Sp)

TABLE III
RUNNING TIMES (S) OF THE PROPOSED PLANT PRODUCTION SYSTEM MONITORING APPLICATION, FOR ALL CONSIDERED DATASETS

	Dictionary pruning	Unmixing		
		SUnSAL (reduced library)	MESMA (reduced library)	MESMA (full library)
January	0.71	189.4	971.8	1.86×10^3
March	0.72	199.2	985.7	1.91×10^3
June	0.71	188.7	927.2	2.22×10^3
September	0.69	187.8	931.6	1.89×10^3

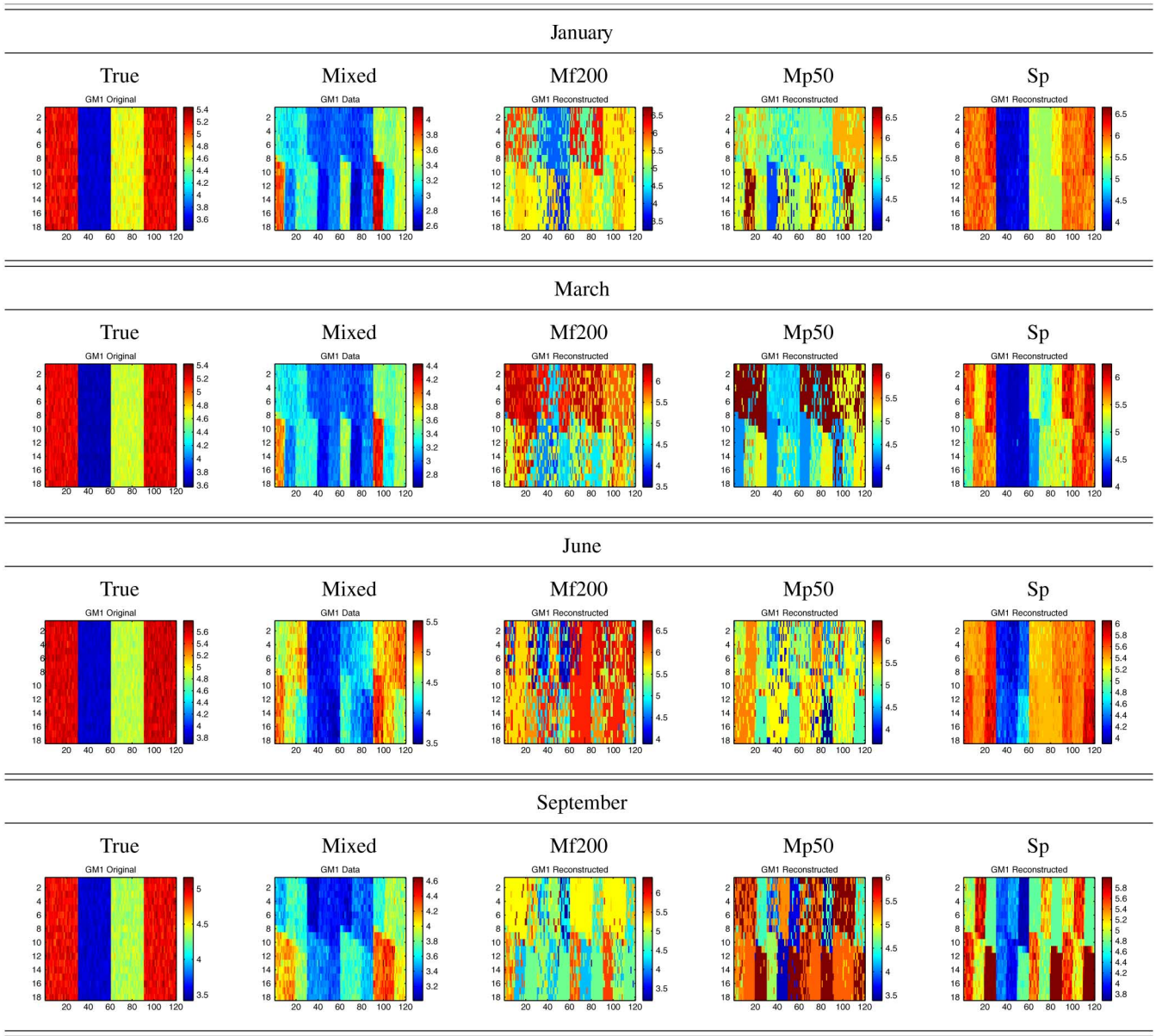

Fig. 8. True and computed GM1 maps in the considered datasets.

(running with optimal parameter λ, infered in Section V-C). On the axis, we mark the spatial position of the pixels in the respective image.

In Figs. 8–10, there are no strong differences visible between the maps produced by MESMA running with the full library and 200 iterations and MESMA running with pruned library and 50 iterations. However, it is important to note that the latter plots were obtained about four times faster than the former ones, due to the corresponding reduction in the number of iterations. On the other hand, SUnSAL appears to perform better than

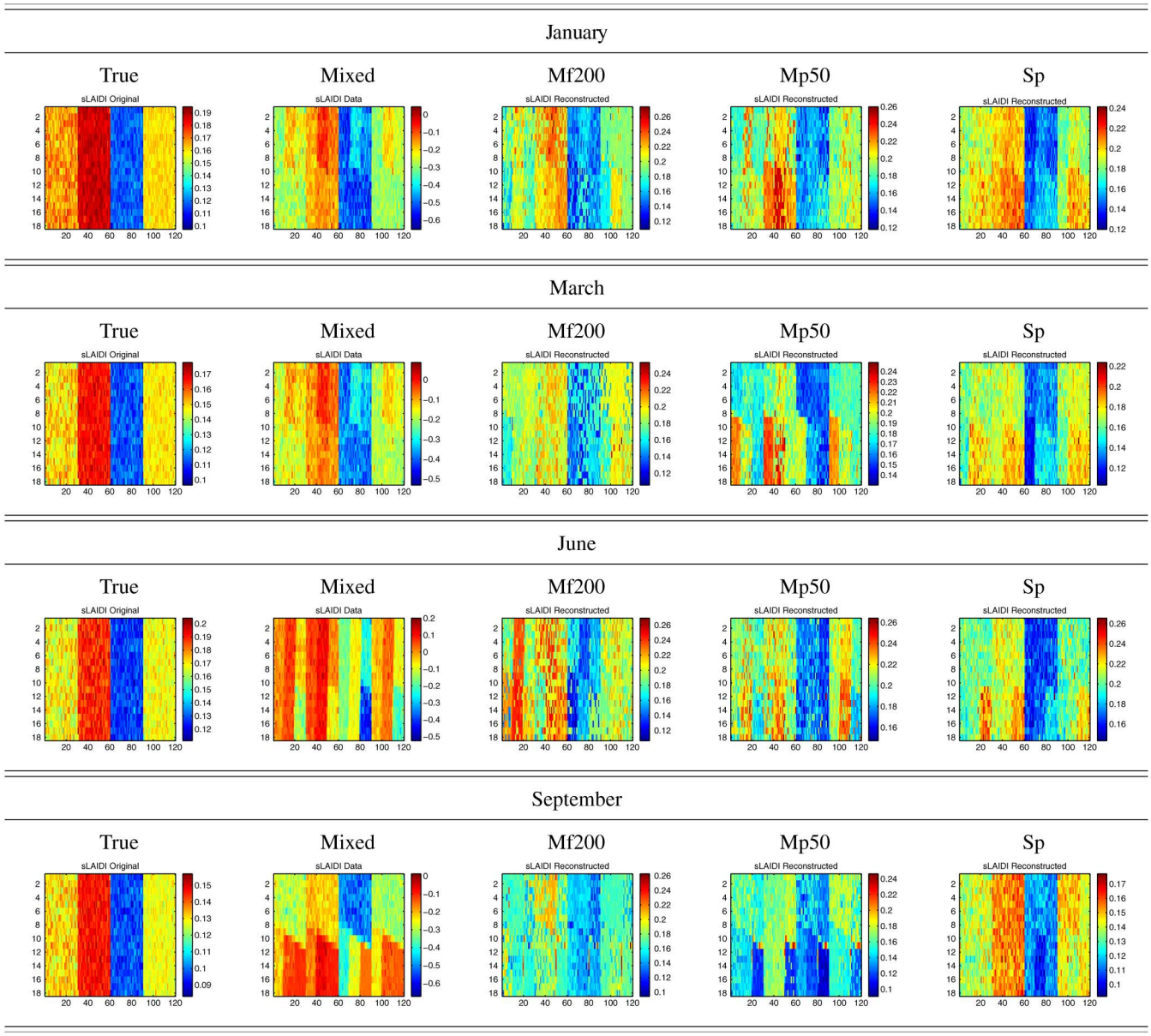

Fig. 9. True and computed sLAIDI maps in the considered datasets.

MESMA in all considered scenarios and all considered vegetation indices.

We are now inspecting the quality of the estimated vegetation indices from a quantitative point of view. In Table IV, we report the ED between the true and estimated vectors correponding to the considered vegetation indices, in all datasets. In Table IV, addition to the cases presented in Figs. 8–10, we include two other cases, for a wider illustration of the achieved performances: estimated vegetation indices using MESMA running with full library and 50 iterations (Mf50) and MESMA running with pruned library and 200 iterations (Mp200).

Table IV confirms the results reported previously. Generally, MESMA running with 200 iterations displays comparable qualities when the two libraries are used, as expected. The use of MESMA with the full library and low number of iterations leads to poor performances. However, the vegetation indices evaluation improves considerably after pruning, for the same number of iterations. Again, SUnSAL shows higher potential than MESMA for the accurate evaluation of the vegetation indices, displaying the lowest ED in all cases, while the indices estimated directly from the observed dataset are least informative, as expected, except for the GM1 index estimated for the June dataset, where only SUnSAL leads to better estimations than the ones obtained directly from the image pixels.

F. Robustness of the Method w.r.t. the Addition of New Signatures in the Spectral Library

In this section, we run a short experiment with the goal to check the sensitiviy of the method w.r.t. to the presence, in the spectral library, of extra signatures which do not contribute to the observed data. In this sense, we extend the spectral library considered in the previous experiments, by including 790 new tree spectral signatures. These signatures were acquired during

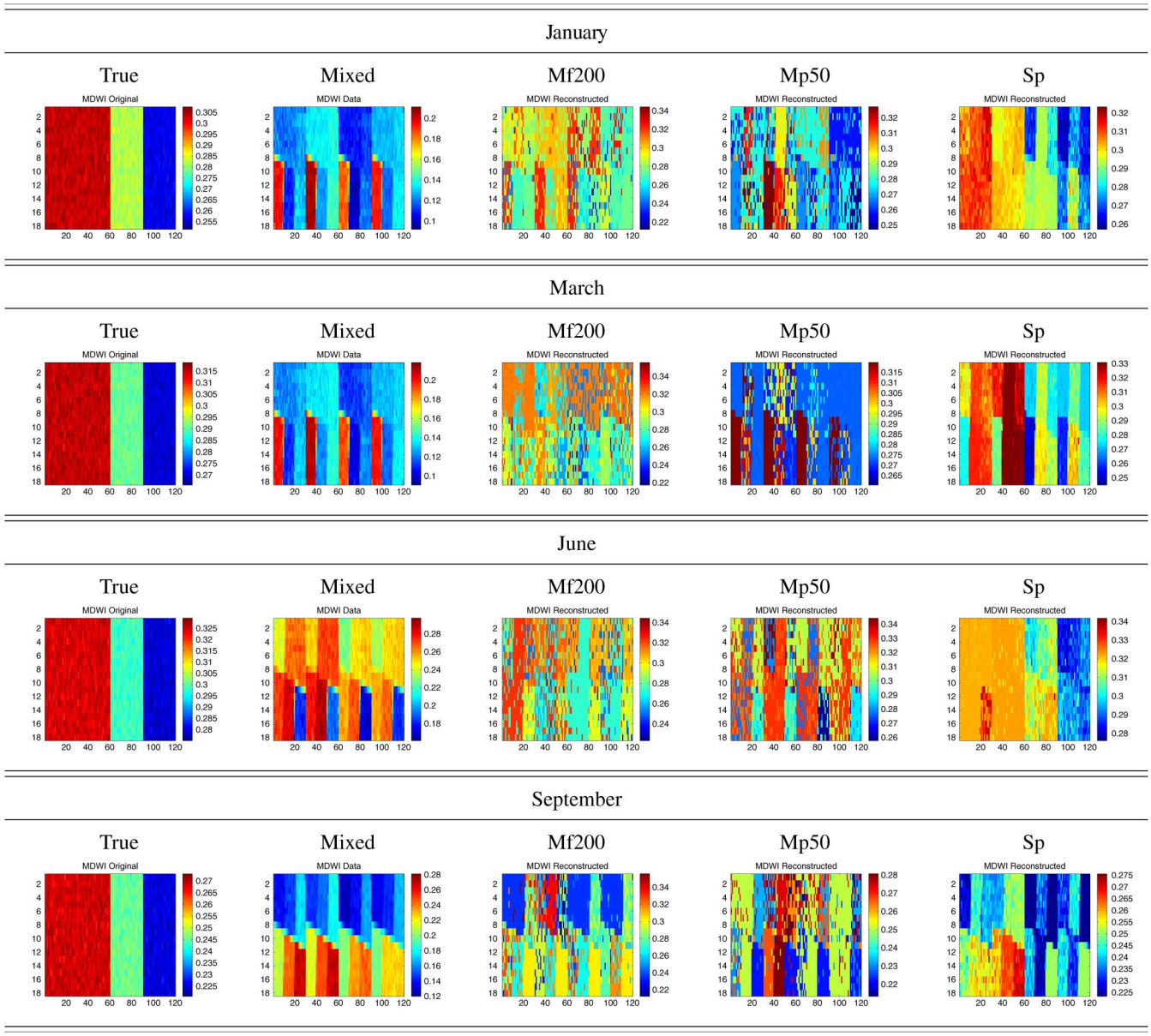

Fig. 10. True and computed MDWI maps in the considered datasets.

TABLE IV
ED BETWEEN TRUE AND ESTIMATED VECTORS OF VEGETATION INDICES IN ALL CONSIDERED DATASETS

		Mixed	Mf200	Mp200	Mf50	Mp50	Sp
January	GM1	74.27	38.41	40.52	46.71	45.43	34.10
	sLAIDI	21.87	1.36	1.35	1.77	1.38	1.36
	MDWI	7.16	1.15	1.09	1.58	0.96	0.58
March	GM1	69.87	47.12	35.06	55.07	40.07	25.02
	sLAIDI	16.46	1.49	1.74	1.46	1.81	1.45
	MDWI	7.55	1.47	1.11	1.63	1.22	0.81
June	GM1	32.52	51.89	40.85	65.81	37.74	17.75
	sLAIDI	11.40	1.50	1.79	1.55	1.68	1.45
	MDWI	3.10	1.35	1.20	1.99	1.31	0.49
September	GM1	40.79	35.86	40.21	45.33	48.66	33.04
	sLAIDI	18.76	1.86	1.27	2.15	1.36	0.50
	MDWI	3.46	2.02	1.30	1.66	1.11	0.87

a period of more than 1 year (September 2008–February 2010) in the same orchard described in Section IV-A. Thus, the new spectral library, which will be denoted by $\mathbf{B}$, contains 3110 spectra with 187 spectral bands. Similar to the plots in Sections V-A and V-B, we plot, in Figs. 11 and 12, the projection errors corresponding to the members of $\mathbf{B}$ and the variability range covered by the selected spectra, respectively, in the considered datasets, when $k_f = k + 35$, $r_1 = 40$, and $r_2 = 540$. The projection errors of the newly added members are highlighted with magenta circles.

Fig. 11 reveals that the added spectra exhibit large projection errors compared to the actual endmembers on the ground, such that none of them is selected in the pruning process. This means that the method is not influenced by the presence of these spectra, which do not contribute to the observed pixels. On the other hand, Fig. 12 shows that, despite the wide range of variability introduced by the enlarged tree spectral library, the pruning

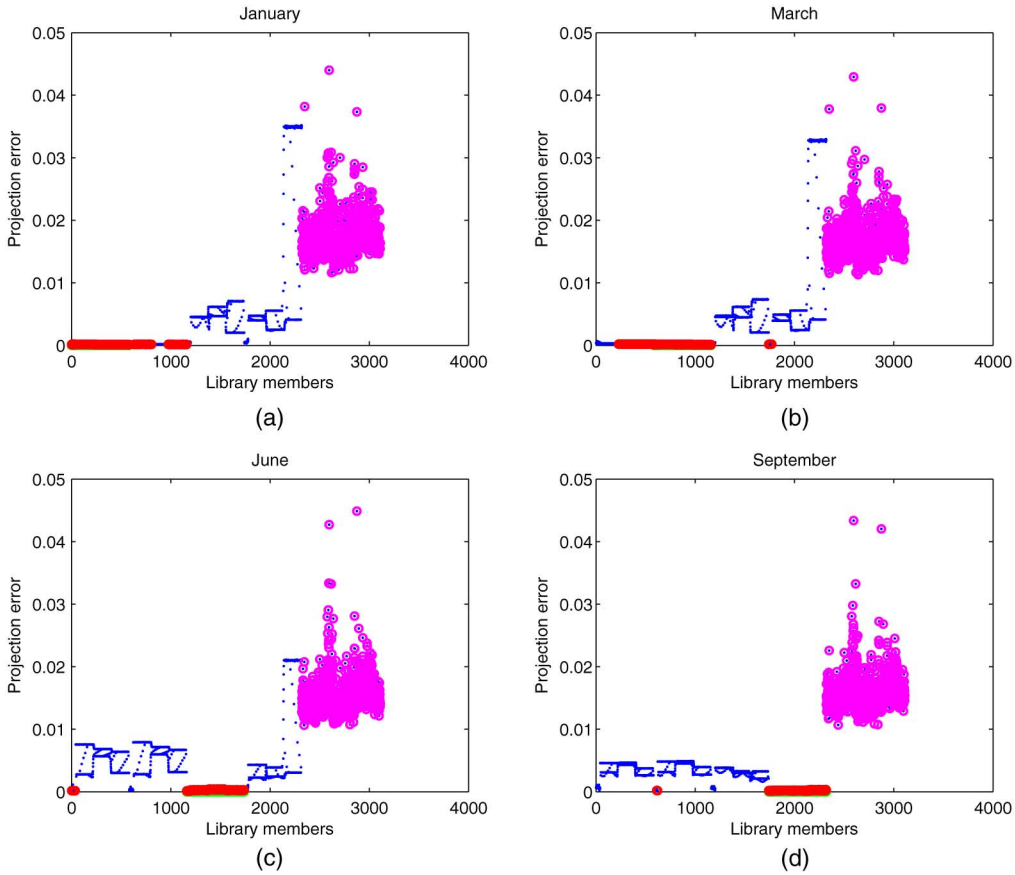

Fig. 11. Projection errors corresponding to each member of $\mathbf{B}$ in the considered datasets. Green circles represent the true endmembers. Red circles correspond to the projection errors of the 580 selected spectra (40 soil spectra and 540 tree spectra). Magenta circles mark the projection errors of the library members added to the original spectra. (a) January, (b) March, (c) June, and (d) September.

method is still able to cover with high accuracy the proper variability range, in the distinct seasons.

The two aforementioned observations prove the robustness of the method to the presence, in the spectral library, of signatures which are not correlated to ground-truth endmembers. In the subsequent unmixing process, it is expected that the results follow the same pattern shown in Section V-C. However, the results obtained with MESMA using the full library $\mathbf{B}$ have a high probability of losing accuracy, for a fixed number of iterations, given that the additional spectra in the library lead to a larger number of possible spectra combinations. This means that, when using the spectral library $\mathbf{B}$, the pruning methodology is able to boost the unmixing performances even more clearly than in the first case analized in the experiments.

G. Discussion on the Obtained Results

From the experimental results presented in this section, a few interesting observations can be drawn. First and foremost, it is important to mention that the dynamic unmixing methodology proposed in this paper is able to provide robust and specific monitoring of plant production systems for a whole year round. Further, the methodology is robust w.r.t. the size of the library and the dimension of the subspace used to define the observed data (the number of eigenvectors retained from the HySime output). We have also shown that, by including new library members, the selection remains stable, which means that, no matter how many extra members are present in the library, the final estimation of vegetation indices does not change significantly. Also, the selected spectra are highly correlated to the actual ones on the ground and they are able to properly cover the full range of variability of the true endmembers. Another observation is that MESMA benefits from pruning in terms of running speed, as it needs less iterations to achieve a certain desired performance. While 50 iterations are never enough to get satisfactory output when the full library is employed, the performances obtained using this relatively low number of iterations and the pruned dictionary compete successfully with the ones obtained with the large library and MESMA running with 200 iterations. However, SUnSAL, the representative algorithm for the sparse unmixing techniques chosen in this work, outperforms MESMA in terms of estimated vegetation indices in all cases. Given that SUnSAL is also much faster than MESMA, we can conclude that sparse unmixing is a powerful alternative in achieving improved monitoring of plant production systems through signal unmixing applications when relying on spectral libraries.

VI. Conclusion and Future Work

In this paper, two major research directions were investigated. A very important novel contribution is the introduction of sparse unmixing techniques as a reliable competitor to common

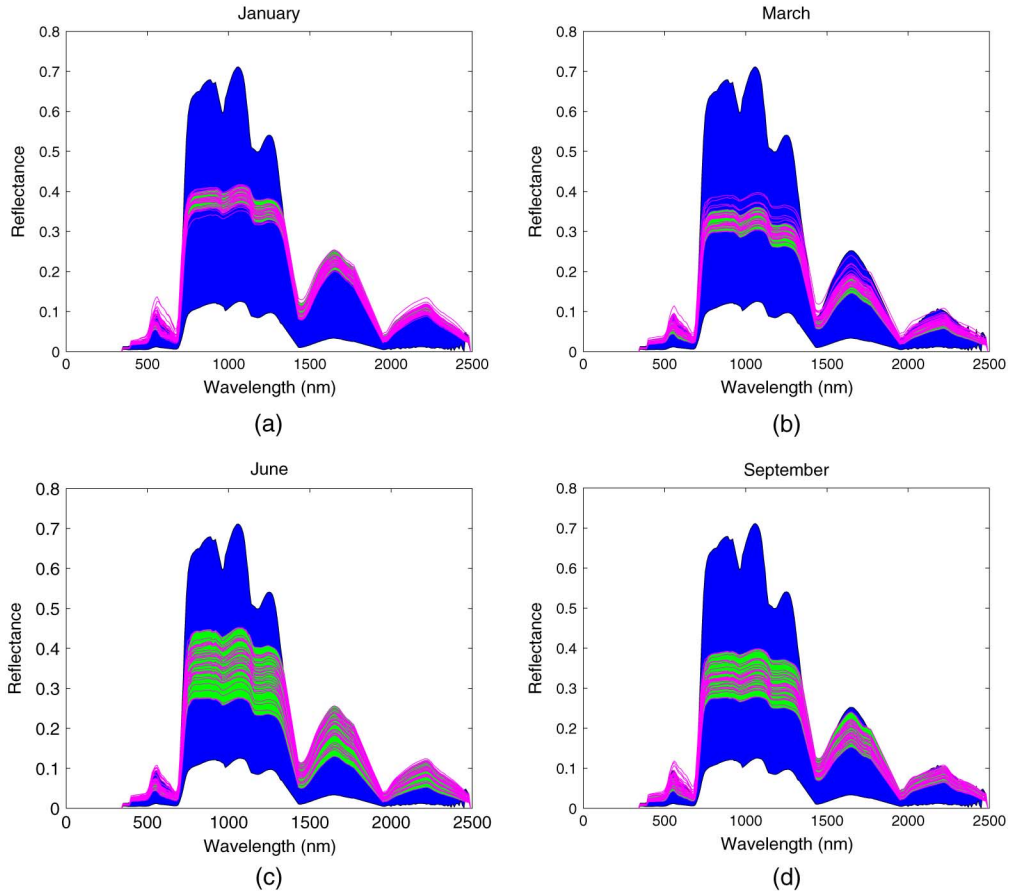

Fig. 12. Quality of the variability range coverage for the four seasons (blue: range of the tree library signatures; green: range of the tree signatures in the specific season; magenta: selected tree signatures through library pruning) when the library $\mathbf{B}$ is employed. (a) January, (b) March, (c) June, and (d) September.

approaches applied in the temporal monitoring of plant production systems. Another important contribution is the exploitation of a dictionary pruning algorithm able to boost the quality of evaluated vegetation indices, when both combinatorial and sparse methods are used. Important improvements over the original method considered, MESMA, were highlighted in a temporal dataset which simulates with high accuracy the variations in vegetation spectra over four seasons, with one representative month for each of them. The experiments also indicated that the dictionary pruning methodology presented here is able to select, with high accuracy, the spectra of the ground-truth endmembers from a large spectral library. Consequently, the quality of the MESMA-based unmixing improves clearly for a low number of iterations. However, our experiments reveal that sparse regression using the pruned dictionary outperforms MESMA both in terms of accuracy of reconstructed spectra and quality of the vegetation indices evaluation. Another important advantage of the considered sparse unmixing technique used in this work, SUnSAL, is related to the running time, which is much lower than that of MESMA.

Future work will focus on the application of the considered methods in a real environment, which was not performed here, as it is very difficult in practice to obtain reliable estimates of ground fractional abundances. The use of simulated spectral libraries, in which the physical characteristics of the corresponding endmembers are known (e.g., water content, chlorophyll content, etc.) is also highly desirable for future experiments. Another future work direction is the exploitation of the (spectral) region based information, in order to analize the influence, in the final unmixing result, of the reflectance values measured in distinct regions of the electromagnetic spectrum. Tests with more heterogeneous environments, in which other endmembers are present (e.g., weeds), will be also conducted. Finally, possible ways to exploit the proposed methodology in diverse large-scale applications using satellite data will be also analyzed.

References

[1] P. Zarco-Tejada, J. Miller, A. Morales, A. Berjon, and J. Aguera, "Hyperspectral indices and model simulation for chlorophyll estimations in open canopy tree crops," *Remote Sens. Environ.*, vol. 90, pp. 463–476, 2004.

[2] K. Richter, C. Atzberger, F. Vuolo, and G. D'Urso, "Evaluation of sentinel-2 spectral sampling for radiative transfer model based LAI estimation of wheat, sugar beet, and maize," *IEEE J. Sel. Topics Appl. Earth Observ. Remote Sens.*, vol. 4, no. 2, pp. 458–464, Jun. 2011.

[3] D. Roberts, M. Smith, and J. Adams, "Green vegetation, nonphotosynthetic vegetation, and soils in AVIRIS data," *Remote Sens. Environ.*, vol. 44, pp. 255–269, 1993.

[4] L. Tits, B. Somers, J. Stuckens, J. Farifteh, and P. Coppin, "Integration of in situ measured soil status and remotely sensed hyperspectral data to improve plant production system monitoring: Concept, perspectives and limitations," *Remote Sens. Environ.*, vol. 128, pp. 197–211, 2013.

[5] D. Lobell and G. Asner, "Cropland distributions from temporal unmixing of MODIS data," *Remote Sens. Environ.*, vol. 93, pp. 412–422, 2004.

[6] D. R. Peddle and A. M. Smith, "Spectral mixture analysis of agricultural crops: Endmember validation and biophysical estimation in potato plots," *Int. J. Remote Sens.*, vol. 26, pp. 4959–4979, 2005.

[7] P. Thenkabail, I. Mariotto, M. Gumma, E. Middleton, D. Landis, and K. Huemmrich, "Selection of hyperspectral narrowbands (HNBs) and composition of hyperspectral twoband vegetation indices (HVIS) for biophysical characterization and discrimination of crop types using field reflectance and hyperion/eo-1 data," *IEEE J. Sel. Topics Appl. Earth Observ. Remote Sens.*, vol. 6, no. 2, pp. 427–439, Apr. 2013.

[8] S. Verbeiren, H. Eerens, I. Piccard, I. Bauwens, and J. V. Orshoven, "Sub-pixel classification of spot-vegetation time series for the assessment of regional crop areas in Belgium," *Int. J. Appl. Earth Obs.*, vol. 10, pp. 486–497, 2008.

[9] A. Huete, "A soil-adjusted vegetation index (SAVI)," *Remote Sens. Environ.*, vol. 25, pp. 295–309, 1988.

[10] F. Baret and G. Guyot, "Potentials and limits of vegetation indexes for LAI and APAR assessment," *Remote Sens. Environ.*, vol. 35, pp. 161–173, 1991.

[11] G. Rondeaux, M. Steven, and F. Baret, "Optimization of soil-adjusted vegetation indices," *Remote Sens. Environ.*, vol. 55, pp. 95–107, 1996.

[12] B. Somers, V. Gysels, W. Verstraeten, S. Delalieux, and P. Coppin, "Modelling moisture-induced soil reflectance changes in cultivated sandy soils: A case study in citrus orchards," *Eur. J. Soil Sci.*, vol. 61, pp. 1091–1105, 2010.

[13] L. Tits, B. Somers, and P. Coppin, "The potential and limitations of a clustering approach for the improved efficiency of multiple endmember spectral mixture analysis in plant production system monitoring," *IEEE Trans. Geosci. Remote Sens.*, vol. 50, no. 6, pp. 2273–2286, Jun. 2012.

[14] D. Roberts, M. Gardner, R. Church, S. Ustin, G. Scheer, and R. Green, "Mapping chaparral in the Santa Monica mountains using multiple endmember spectral mixture models," *Remote Sens. Environ.*, vol. 65, no. 3, pp. 267–279, 1998.

[15] M.-D. Iordache, J. Bioucas-Dias, and A. Plaza, "Unmixing sparse hyperspectral mixtures," in *Proc. IEEE Int. Geosci. Remote Sens. (IGARSS)*, Cape Town, South Africa, 2009, pp. 85–88.

[16] M.-D. Iordache, J. Bioucas-Dias, and A. Plaza, "Sparse hyperspectral unmixing," in *Proc. 6th EARSeL SIG IS Workshop*, Tel Aviv, Israel, Mar. 2009, vol. 1, pp. 1–4.

[17] M.-D. Iordache, "*A sparse regression approach to hyperspectral unmixing*," Ph.D. dissertation, Inst. Superior Tecnico, TULisbon, Lisbon, Portugal, 2011. [Online] Available: http://www.lx.it.pt/bioucas/files/PhD_Daniel_sparse_regression_2011.pdf

[18] J. Eckstein and D. Bertsekas, "On the Douglas–Rachford splitting method and the proximal point algorithm for maximal monotone operators," *Math. Program.*, vol. 5, pp. 293–318, 1992.

[19] J. Bioucas-Dias and M. Figueiredo, "Alternating direction algorithms for constrained sparse regression: Application to hyperspectral unmixing," in *Proc. 2nd IEEE GRSS Workshop Hyperspectral Image Signal Process.: Evol. Remote Sens. (WHISPERS)*, Reykjavik, Iceland, 2010, vol. 1, pp. 1–4.

[20] M.-D. Iordache, J. Bioucas-Dias, and A. Plaza, "Sparse unmixing of hyperspectral data," *IEEE Trans. Geosci. Remote Sens.*, vol. 49, no. 6, pp. 2014–2039, Jun. 2011.

[21] J. M. Bioucas-Dias, A. Plaza, N. Dobigeon, M. Parente, Q. Du, P. Gader *et al.*, "Hyperspectral unmixing overview: Geometrical, statistical and sparse regression-based approaches," *IEEE J. Sel. Topics Appl. Earth Observ. Remote Sens.*, vol. 5, no. 2, pp. 354–379, Apr. 2012.

[22] B. Somers, M. Zortea, A. Plaza, and G. Asner, "Automated extraction of image-based endmember bundles for improved spectral unmixing," *IEEE J. Sel. Topics Appl. Earth Observ. Remote Sens.*, vol. 5, no. 2, pp. 396–408, Apr. 2012.

[23] J. Price, "How unique are spectral signatures?," *Remote Sens. Environ.*, vol. 49, pp. 181–186, 1994.

[24] J. Boardman, F. Kruse, and R. Green, "Mapping target signatures via partial unmixing of AVIRIS data," in *Proc. 5th JPL Airborne Earth Sci. Workshop*, Pasadena, CA, USA, 1995, pp. 23–26.

[25] P. Dennison and D. Roberts, "Endmember selection for multiple endmember spectral mixture analysis using endmember average RMSE," *Remote Sens. Environ.*, vol. 87, pp. 123–135, 2003.

[26] S. Tompkins, J. Mustard, C. Pieters, and D. Forsyth, "Optimization of endmembers for spectral mixture analysis," *Remote Sens. Environ.*, vol. 59, pp. 472–489, 1997.

[27] A. Schaaf, P. Dennison, G. Fryer, K. Roth, and D. Roberts, "Mapping plant functional types at three spatial resolutions using multiple endmember spectral mixture analysis," *GISci. Remote Sens.*, vol. 48, pp. 324–344, 2011.

[28] B. Somers, G. Asner, L. Tits, and P. Coppin, "Endmember variability in spectral mixture analysis: A review," *Remote Sens. Environ.*, vol. 115, no. 7, pp. 1603–1616, Jul. 2011.

[29] D. Anderson and A. Zare, "Spectral unmixing cluster validity index for multiple sets of endmembers," *IEEE J. Sel. Topics Appl. Earth Observ. Remote Sens.*, vol. 5, no. 4, pp. 1282–1295, Aug. 2012.

[30] K. Roth, P. Dennison, and D. Roberts, "Comparing endmember selection techniques for accurate mapping of plant species and land cover using imaging spectrometer data," *Remote Sens. Environ.*, vol. 127, pp. 139–152, 2012.

[31] P. Pinter, J. Hatfield, J. Schepers, E. Barnes, M. Moran, C. Daughtry, and D. Upchurch, "Remote sensing for crop management," *Photogramm. Eng. Remote Sens.*, vol. 69, no. 6, pp. 647–664, Jun. 2003.

[32] M.-D. Iordache, J. Bioucas-Dias, A. Plaza, and B. Somers, "MUSIC-CSR: Hyperspectral unmixing via multiple signal classification and collaborative sparse regression," *IEEE Trans. Geosci. Remote Sens.*, vol. 52, no. 7, pp. 4364–4382, Jul. 2014.

[33] M.-D. Iordache, J. M. Bioucas-Dias, and A. Plaza, "Dictionary pruning in sparse unmixing of hyperspectral data," in *Proc. 4th IEEE GRSS Workshop Hyperspectral Image Signal Process.: Evol. Remote Sens. (WHISPERS)*, Shanghai, China, 2012, vol. 1, pp. 1–4.

[34] D. Heinz and C.-I. Chang, "Fully constrained least squares linear mixture analysis for material quantification in hyperspectral imagery," *IEEE Trans. Geosci. Remote Sens.*, vol. 39, no. 3, pp. 529–545, Mar. 2001.

[35] A. Bruckstein, D. Donoho, and M. Elad, "From sparse solutions of systems of equations to sparse modeling of signals and images," *Review*, vol. 51, pp. 34–81, 2009.

[36] A. Bruckstein, M. Elad, and M. Zibulevsky, "On the uniqueness of nonnegative sparse solutions to underdetermined systems of equations," *IEEE Trans. Inf. Theory*, vol. 54, no. 11, pp. 4813–4820, Nov. 2008.

[37] E. Candès, J. Romberg, and T. Tao, "Stable signal recovery from incomplete and inaccurate measurements," *Commun. Pure Appl. Math.*, vol. 59, no. 8, p. 1207, 2006.

[38] E. Candès and T. Tao, "Decoding by linear programming," *IEEE Trans. Inf. Theory*, vol. 51, no. 12, pp. 4203–4215, Dec. 2005.

[39] B. Natarajan, "Sparse approximate solutions to linear systems," *SIAM J. Comput.*, vol. 24, no. 2, pp. 227–234, 1995.

[40] J. Tropp, "*Just relax: Convex programming methods for subset selection and sparse approximation*," *IEEE Trans. Inf. Theory*, vol. 52, no. 3, pp. 1030–1051, 2006.

[41] S. Chen, D. Donoho, and M. Saunders, "Atomic decomposition by basis pursuit," *SIAM Rev.*, vol. 43, no. 1, pp. 129–159, 2001.

[42] Y. Pati, R. Rezahfar, and P. Krishnaprasad, "Orthogonal matching pursuit: Recursive function approximation with applications to wavelet decomposition," in *Proc. 27th IEEE Asilomar Conf. Signals Syst. Comput. (ASSC)*, Los Alamitos, CA, USA, 2003, pp. 40–44.

[43] D. Rogge, B. Rivard, J. Zhang, and J. Feng, "Iterative spectral unmixing for optimizing per-pixel endmember sets," *IEEE Trans. Geosci. Remote Sens.*, vol. 44, no. 12, pp. 3725–3736, Dec. 2006.

[44] M.-D. Iordache, J. Bioucas-Dias, and A. Plaza, "Hyperspectral unmixing with sparse group lasso," in *Proc. IEEE Int. Conf. Geosci. Remote Sens. (IGARSS)*, 2011, pp. 3586–3589.

[45] M.-D. Iordache, J. Bioucas-Dias, and A. Plaza, "Collaborative sparse regression for hyperspectral unmixing," *IEEE Trans. Geosci. Remote Sens.*, vol. 52, no. 1, pp. 341–354, Jan. 2014.

[46] M.-D. Iordache, J. Bioucas-Dias, and A. Plaza, "Total variation spatial regularization for sparse hyperspectral unmixing," *IEEE Trans. Geosci. Remote Sens.*, vol. 50, no. 11, pp. 4484–4502, Nov. 2012.

[47] X.-L. Zhao, F. Wang, T.-Z. Huang, M. Ng, and R. Plemmons, "Deblurring and sparse unmixing for hyperspectral images," *IEEE Trans. Geosci. Remote Sens.*, vol. 51, no. 7, pp. 4045–4058, Jul. 2013.

[48] R. Schmidt, "Multiple emitter location and signal parameter estimation," *IEEE Trans. Antennas Propag.*, vol. 34, no. 3, pp. 276–280, Mar. 1986.

[49] G. Bienvenu and L. Kopp, "Adaptivity to background noise spatial coherence for high resolution passive methods," in *Proc. IEEE Int. Conf. Acoust. Speech Signal Process. (ICASSP)*, 1980, vol. 5, pp. 307–310.

[50] J. Bioucas-Dias and J. Nascimento, "Hyperspectral subspace identification," *IEEE Trans. Geosci. Remote Sens.*, vol. 46, no. 8, pp. 2435–2445, Aug. 2008.

[51] J. Stuckens, B. Somers, S. Delalieux, W. Verstraeten, and P. Coppin, "The impact of common assumptions on canopy radiative transfer simulations: A case study in citrus orchards," *J. Quant. Spectrosc. Radiat.*, vol. 110, pp. 1–21, 2009.

[52] M. Pharr and G. Humphreys, *Physically Based Rendering: From Theory to Implementation*. San Mateo, CA, USA: Morgan Kaufmann, 2004.

[53] J. Weber and J. Penn, "Creation and rendering of realistic trees," in *Proc. 22nd Ann. Conf. Comput. Graphics Interactive Techn.*, Los Angeles, CA, USA, 1995, pp. 119–128.

[54] J. Stuckens, S. Dzikiti, W. Verstraeten, S. Verreynne, R. Swennen, and P. Coppin, "Physiological interpretation of a hyperspectral time series in a citrus orchard," *Agric. Forest Meteorol.*, vol. 151, no. 7, pp. 1002–1015, Jul. 2011.

[55] S. Jacquemoud and F. Baret, "Prospect: A model of leaf optical properties spectra," *Remote Sens. Environ.*, vol. 34, pp. 75–91, 1990.

[56] A. Gitelson and M. Merzlyak, "Signature analysis of leaf reflectance spectra: Algorithm development for remote sensing of chlorophyll," *J. Plant Physiol.*, vol. 148, pp. 494–500, 1996.
[57] S. Delalieux, B. Somers, S. Hereijgers, W. Verstraeten, W. Keulemans, and P. Coppin, "A near-infrared narrow-waveband ratio to determine leaf area index in orchards," *Remote Sens. Environ.*, vol. 68, pp. 3762–3772, 2008.
[58] J. Eitel, P. Gessler, A. Smith, and R. Robberecht, "Suitability of existing and novel spectral indices to remotely detect water stress in populus spp," *Forest Ecol. Manage.*, vol. 229, pp. 170–182, 2006.
[59] P. Zarco-Tejada, J. Miller, A. Morales, A. Berjon, and J. Aguera, "Hyperspectral indices and model simulation for chlorophyll estimations in open canopy tree crops," *Remote Sens. Environ.*, vol. 90, pp. 463–476, 2004.
[60] S. Dzikiti, J. Verreynne, J. Stuckens, A. Strever, W. Verstraeten, and R. Swennen, "Determining the water status of Satsuma mandarin trees [Citrus Unshiu Marcovitch] using spectral indices and by combining hyperspectral and physiological data," *Agric. Forest Meteorol.*, vol. 150, pp. 369–379, 2010.
[61] B. Somers, S. Delalieux, W. Verstraeten, and P. Coppin, "A conceptual framework for the simultaneous extraction of sub-pixel spatial extent and spectral characteristics of crops," *Photogramm. Eng. Remote Sens.*, vol. 75, pp. 57–68, 2009.

Marian-Daniel Iordache received the M.Sc. degree from the Faculty of Electrical Engineering, Politehnica University of Bucharest, Bucharest, Romania, in 2006, and the Ph.D. degree in electrical and computer engineering from Instituto Superior Tecnico, Lisbon, Portugal, in 2011.

His research activity started in 2006 at the Electrical Engineering Research Center, Bucharest, where he worked on several national and European projects dedicated to microelectromechanical systems and high-frequency circuits. From 2008 to 2011, he was a Marie Curie Fellow with the Hyperspectral Imaging Network project funded by the European Commission under the Sixth Framework Programme. He is currently carrying out his research as a researcher and image processing scientist at the Flemish Institute for Technological Research, Center for Remote Sensing and Earth Observation Processes (TAP), Mol, Belgium. His research interest includes hyperspectral unmixing, with emphasis on the sparse characteristics of the solutions.

Dr. Iordache is a member of the Hyperspectral Computing Laboratory research group, University of Extremadura, Cáceres, Spain, since 2010. For his research activity and social implication, he was awarded with the prize *The Romanian Student of the Year in Europe 2011*, offered by the League of Romanian Students Abroad. He is serving as a Reviewer for more than 10 international peer-reivewed international journals, such as IEEE TRANSACTIONS ON GEOSCIENCE AND REMOTE SENSING, IEEE JOURNAL OF SELECTED TOPICS IN APPLIED EARTH OBSERVATIONS IN REMOTE SENSING, IEEE TRANSACTIONS ON SIGNAL PROCESSING, IEEE-TRANSACTIONS ON SYSTEMS, MAN, AND CYBERNETICS, *Optics Express*, among others.

Laurent Tits received the M.Sc. and Ph.D. degrees in bioscience engineering (land and forest management) from the KU Leuven, Belgium, in 2009 and 2013, respectively.

Since 2010, he has been a Research Assistant at the Geomatics Engineering Group, Department of Biosystems, KU Leuven, Leuven, Belgium. His research interests include hyperspectral as well as thermal remote sensing in vegetative systems, with a specific focus on spectral and thermal mixture analysis.

José M. Bioucas-Dias (S'87, M'95) received the E.E., M.Sc., Ph.D., and "Agregado" degrees in electrical and computer engineering from Instituto Superior Técnico (IST), the engineering school of the Technical University of Lisbon (TULisbon), Portugal, in 1985, 1991, 1995, and 2007, respectively.

Since 1995, he has been with the Department of Electrical and Computer Engineering, IST, where he was an Assistant Professor from 1995 to 2007 and an Associate Professor since 2007. Since 1993, he is also a Senior Researcher with the Pattern and Image Analysis group of the Instituto de Telecomunicações, which is a private nonprofit research institution. His research interests include inverse problems, signal and image processing, pattern recognition, optimization, and remote sensing.

Dr. Bioucas-Dias has authored or co-authored more than 230 scientific publications including more than 60 journal papers (48 of them published in IEEE journals) and 170 peer-reviewed international conference papers and book chapters. He was an Associate Editor for the IEEE TRANSACTIONS ON CIRCUITS AND SYSTEMS (1997–2000) and he is an Associate Editor for the IEEE TRANSACTIONS ON IMAGE PROCESSING and IEEE TRANSACTIONS ON GEOSCIENCE AND REMOTE SENSING. He was a Guest Editor of IEEE TRANSACTIONS ON GEOSCIENCE AND REMOTE SENSING for the *Special Issue on Spectral Unmixing of Remotely Sensed Data*, of IEEE JOURNAL OF SELECTED TOPICS IN APPLIED EARTH OBSERVATIONS AND REMOTE SENSING for the *Special Issue on Hyperspectral Image and Signal Processing*, and of IEEE SIGNAL PROCESSING MAGAZINE for the *Special Issue on Signal and Image Processing in Hyperspectral Remote Sensing*. He was the General Co-Chair of the 3rd IEEE GRSS Workshop on Hyperspectral Image and Signal Processing, Evolution in Remote sensing (WHISPERS'2011) and has been a member of program/technical committees of several international conferences.

Antonio Plaza (M'05– SM'07) is an Associate Professor (with accreditation for Full Professor) with the Department of Technology of Computers and Communications, University of Extremadura, where he is the Head of the Hyperspectral Computing Laboratory (HyperComp).

He was the Coordinator of the Hyperspectral Imaging Network, a European project with total funding of 2.8 MEuro. He authored more than 400 publications, including more than 110 JCR journal papers (66 in IEEE journals), 20 book chapters, and over 240 peer-reviewed conference proceeding papers (94 in IEEE conferences). He has guest edited seven special issues on JCR journals (three in IEEE journals). He has been a Chair for the IEEE Workshop on Hyperspectral Image and Signal Processing: Evolution in Remote Sensing (2011).

Dr. Plaza is a recipient of the recognition of Best Reviewers of the IEEE GEOSCIENCE AND REMOTE SENSING LETTERS (in 2009) and a recipient of the recognition of Best Reviewers of the IEEE TRANSACTIONS ON GEOSCIENCE AND REMOTE SENSING (in 2010), a journal for which he has served as Associate Editor in 2007–2012. He is also an Associate Editor for IEEE ACCESS and the IEEE GEOSCIENCE AND REMOTE SENSING MAGAZINE, and was a member of the Editorial Board of the IEEE GEOSCIENCE AND REMOTE SENSING NEWSLETTER (2011–2012) and a member of the steering committee of the IEEE JOURNAL OF SELECTED TOPICS IN APPLIED EARTH OBSERVATIONS AND REMOTE SENSING (2012). He served as the Director of Education Activities for the IEEE Geoscience and Remote Sensing Society (GRSS) in 2011–2012, and is currently serving as President of the Spanish Chapter of IEEE GRSS (since November 2012). He is currently serving as the Editor-in-Chief of the IEEE TRANSACTIONS ON GEOSCIENCE AND REMOTE SENSING JOURNAL (since January 2013).

Ben Somers was born in Leuven, Belgium, on September 13, 1982. He received the M.Sc. and Ph.D. degrees in bioscience engineering (land and forest management) from the Katholieke Universiteit Leuven (KU Leuven), Belgium, in 2005 and 2009, respectively.

In 2010, he was research associate at the Geomatics Engineering group of the KU Leuven. From 2011 to 2013, he was researcher at the Remote Sensing division of the Flemish Institute for Technological Research (VITO), Belgium. In October 2013, he started as an Assistant Professor (tenure track position) at the Division Forest, Nature & Landscape of the Department of Earth & Environmental Sciences of the KU Leuven. He is experienced in the design and integration of state-of-the-art remote sensing techniques to study the impact of disturbance processes (nutrient deficiencies, pests and diseases, invasive exotic species, climate change) on the functioning of terrestrial ecosystems. His current research is focused on fostering the use and application of remote sensing in support of sustainable management of (semi)natural and urban environments.